# Kinetic control on Zn isotope signatures recorded in marine diatoms

# Kinetic control on Zn isotope signatures recorded in marine diatoms

**Michael Köbberich*** **and Derek Vance**

*To whom correspondence should be addressed

Submitted to: ***Geochimica et Cosmochimica Acta***

## Affiliation

Institute of Geochemistry and Petrology
Department of Earth Sciences, ETH Zurich
Clausiusstrasse 25 , NW C 81.1
CH-8092 Zurich, Switzerland
michael.koebberich@erdw.ethz.ch

## Running head

Kinetic control on diatom Zn isotopes

# Abstract

Marine diatoms dominate the oceanic cycle of the essential micronutrient zinc (Zn). The stable isotopes of zinc and other metals are increasingly used to understand trace metal micronutrient cycling in the oceans. One clear feature of the early isotope data is the heavy Zn isotope signature of the average oceanic dissolved pool relative to the inputs, potentially driven by uptake of light isotopes into phytoplankton cells and export to sediments. However, despite the fact that diatoms strip Zn from surface waters across the Antarctic polar front in the Southern Ocean, the local upper ocean is not isotopically heavy. Here we use culturing experiments to quantify the extent of Zn isotope fractionation by diatoms and to elucidate the mechanisms driving it.

We have cultured two different open-ocean diatom species (*T. oceanica* and *Chaetoceros sp.*) in a series of experiments at constant medium Zn concentration but at bioavailable medium Fe ranging from limiting to replete. We find that *T. oceanica* can maintain high growth rates and Zn uptake rates over the full range of bioavailable iron (Fe) investigated, and that the Zn taken up has a $\delta^{66}$Zn that is unfractionated relative to that of the bioavailable free Zn in the medium. The studied representative of the genus *Chaetoceros*, on the other hand, shows more significantly reduced Zn uptake rates at low Fe and records more variable biomass $\delta^{66}$Zn signatures, of up to 0.85 ‰ heavier than the medium. We interpret the preferential uptake of heavy isotopes at extremely low Zn uptake rates as potentially due to either of the following two mechanisms. First, the release of extracellular polymeric substances (EPS), at low Fe levels, may preferentially scavenge heavy Zn isotopes. Second, the Zn uptake rate may be slow enough to establish pseudo-equilibrium conditions at the transporter site, with heavy Zn isotopes forming more stable surface complexes.

Thus we find that, in our experiments, Fe-limitation exerts a key control that not only limits diatom growth, but also affects the Zn uptake physiology of diatoms. Uptake of heavy isotopes occurs under Fe-limiting conditions that drive extremely low Zn uptake rates. On the other hand, more rapid Zn uptake rates result in biomass that is indistinguishable from the external bioavailable free Zn pool. These experimental results can, in principle, explain the range of Zn

47 isotopic compositions found in the real surface ocean, given the geographically variable interplay
48 between Fe-limitation, Zn uptake rates, and the degree of organic complexation of oceanic Zn.

# 1. Introduction

Transition metals, such as zinc (Zn) and iron (Fe), show nutrient-like depth profiles in the ocean, characterized by extreme photic zone depletion and deep enrichment (*e.g.* Bruland, 1980; Martin et al., 1989). Zn cellular abundances exceed those of Fe in a key phytoplankton group, the diatoms (Morel et al., 2003; Twining and Baines, 2013). The jury is still out, however, on whether Zn concentrations in the photic zone of the oceans are ever low enough to limit phytoplankton growth (*e.g.* Crawford et al., 2003; Moore et al., 2013), as has been found to be the case for Fe in high nutrient low chlorophyll (HNLC) zones like the Southern Ocean (see review by Boyd and Ellwood, 2010).

Recently, stable isotope systems have begun to be harnessed as tools in attempts to understand the oceanic distributions of transition metals and in particular their participation in biogeochemical cycles (*e.g.* Bermin et al., 2006; Abouchami et al., 2011; Conway and John, 2014b, a; John and Conway, 2014; Zhao et al., 2014; Conway and John, 2015a, b). For Zn, the focus here, some important first-order features of the stable isotope distributions are emerging. The first is that Zn stable isotopes exhibit remarkable homogeneity beneath the permanent thermocline, with $\delta^{66}Zn_{\text{JMC 3-0749}}$ around +0.5 ‰. This isotopic composition is slightly but significantly heavier than the known inputs to the oceans, but much lighter than some of the well-characterized sedimentary outputs, such as those associated with Fe-Mn oxides, as well as carbonate and opaline sediments (Little et al., 2014). Recent findings of isotopically light authigenic Zn in organic-rich sediments (Little et al., 2016) could resolve the implied imbalance, but the extent to which this light output is driven by uptake of isotopically light Zn in the photic zone during photosynthesis versus diagenetic fixation of light Zn in sulfide within the sediment is currently debated (Little et al., 2016; Vance et al., 2016a).

The variability that has been observed to date in the dissolved pool is confined to the upper ocean, consistent with biological cycling exerting an important control on oceanic Zn isotopes. However, within the surface ocean, an important difference has emerged. In the low latitude Atlantic, Zn isotopes show a shift towards lighter values in waters of the upper ocean (Conway

and John, 2014a). By contrast, the surface Southern Ocean shows remarkably constant Zn isotope compositions (Zhao et al., 2014; Archer et al., 2016). This homogeneity in Zn occurs despite the fact that dissolved Zn concentrations drop by about a factor of 40 moving away from the upwelling zone in the Antarctic zone of the Southern Ocean, as water is rapidly depleted in nutrients in the Ekman flow northwards to the sub-Antarctic (Wyatt et al., 2014; Zhao et al., 2014).

There are a number of factors that might explain this important difference between the Southern Ocean and other parts of the global ocean. The first is that the ecology of the Southern Ocean is dominated by fast-growing diatoms (*e.g.* Armbrust, 2009). Marine diatoms not only account for as much as 40 % of oceanic $CO_2$ fixation (Armbrust et al., 2004), but also appear to be responsible for more than half of export production, that portion of primary production that escapes recycling in the photic zone (Smetacek et al., 2012). Given that Southern Ocean diatoms exhibit particularly high cellular Zn contents, with phosphate-normalized Zn abundances that are up to a factor of 10 higher than average oceanic phytoplankton (Twining and Baines, 2013), this region and these organisms must be key to the isotopic character of the biogenic output of Zn to sediment (Vance et al., 2017).

Other features of the Southern Ocean are potentially relevant here. Over most of the photic zone of the global oceans, Zn in seawater solutions is predominantly complexed by organic ligands, with only a small fraction of the dissolved pool existing as the bioavailable $Zn^{2+}$ species (*e.g.* Bruland, 1989; Donat and Bruland, 1990; Ellwood and Van den Berg, 2000; Ellwood, 2004; Lohan et al., 2005). The Southern Ocean is the only location as yet known where total dissolved Zn is in excess of the ligand concentration, so that the bioavailable $Zn^{2+}$ concentration is high (Baars and Croot, 2011). Moreover, chronic Fe-limitation in the Southern Ocean might exert a key control that not only limits diatom growth, but might also affect the Zn uptake physiology of diatoms.

The aim of this contribution is to explore these issues using a culturing approach. In particular, we seek to investigate the reasons why diatoms in the Fe-limited Southern Ocean display their

distinctive characteristics in terms of uptake stoichiometry and Zn isotope systematics. To our knowledge, *Thalassiosira oceanica* is thus far the only marine diatom for which Zn isotope behavior during uptake has been studied (John et al., 2007), though there is a significant amount of information on the processes controlling *elemental* uptake patterns (see Section 2). Important environmental factors that may be relevant in the real ocean, such as, for example, the impact of external growth limiting factors such as low Fe concentrations, have not been explored. Specifically, here, we document Zn isotope systematics during uptake for another diatom species. Secondly, we seek to elucidate the physiological interplay between Zn and Fe uptake with respect to the distribution of Zn isotopes during uptake into cultured marine diatoms of two different species. Third, we aim to set the isotopic data in the context of variation in cellular Zn quotas, with particular emphasis on the variability of Zn/P ratios with decreasing Fe concentrations.

## 2. Background

The processes controlling uptake of micronutrient metals by phytoplankton have been studied in culture for three decades (*e.g.* Morel et al., 1979; Sunda and Huntsman, 1992, 1995b, 1997; Lis et al., 2015), and this work serves as a launching pad for the stable isotope work detailed in this contribution. It has long been known that the uptake of metals such as Fe by marine phytoplankton is controlled by the availability of an inorganically bound, unchelated, pool, denoted Fe′ (Sunda and Huntsman, 1997; Shaked et al., 2005; Shaked and Lis, 2012). In culturing experiments, this bioavailable pool of all non-organically bound 'free metals' is commonly kept at constant and low levels over the duration of the experiments using a transition metal buffer, typically strong organic chelators (Anderson and Morel, 1982; Sunda et al., 2005). The fact that the relationship between Fe′ and uptake rate holds only for surface area normalized rates (Sunda and Huntsman, 1995b, 1997; Lis et al., 2015) suggests that diatoms regulate their Fe uptake *e.g.* by modifying the number of transport proteins actively carrying metals across the cell wall. The light-induced dissociation of the Fe-EDTA complex (Sunda and Huntsman, 2003) and an extracellular Fe reduction step (Shaked et al., 2005) are further important influences on Fe uptake rates in culture.

In the case of Zn, available knowledge goes beyond the simple observation that uptake rates correlate with the bioavailable Zn′ concentration. There is, for instance, evidence for at least two different uptake mechanisms, high- and low-affinity pathways (Sunda and Huntsman, 1992), previously suggested to cause different isotope effects (John et al., 2007). Whereas the first is active over the entire range of naturally occurring bioavailable Zn concentrations, an additional mechanism, which becomes active at Zn levels above the saturation level of the first pathway, may be able to further increase uptake. Previous research has also suggested that the binding rate to cell wall transporters is related to the water loss rate for the reacting aqueous species, and is thus largely independent of the chemical nature of the membrane transporter site (Hudson and Morel, 1990; Hudson, 1998; Sunda and Huntsman, 1998). In other words, the rate-limiting step in the entire Zn uptake kinetics, from the transition metal buffer to the inside of the diatom, is the formation of an inner-sphere from an outer-sphere complex at the membrane transporter (Figure 1). Although such rate constants are important for marine life, their numerical values have not usually been measured, but theoretically predicted (Hudson and Morel, 1990). Stable metal isotopes offer an opportunity to quantitatively explore the molecular basis behind such uptake mechanisms.

# 3. Materials & Methods

Only ultrapure water, with a conductivity of 18.2 MΩ·cm, was used in this study and came from a Milli-Q® integral water purification system (Merck, Millipore, Germany). Reagent grade acids were twice purified by sub-boiling distillation (DST-1000, Savillex, USA). All salts used for the preparation of artificial seawater solutions were either of trace metal purity, or solutions made from them were cleaned using a chelating resin (Chelex® 100, Bio-Rad, USA). Handling of all reagents, solutions, and phytoplankton cultures was carried out under ‘Class 100’ clean laboratory conditions at constant humidity of around 10 % and a temperature of 21.2 ± 0.2 °C.

### 3.1 Artificial seawater medium

The artificial medium used in this study was designed to allow variation of the bioavailable Fe′ concentration from conditions that yield maximum growth of the studied organism down to those that significantly limit growth. The maximum inorganic Fe (Fe′) concentration used was high enough to achieve intense growth and low enough to avoid the precipitation of extra Fe onto diatom surfaces (Sunda and Huntsman, 1995b, 1997). Since the principle aim here is to investigate the variation in Zn uptake and isotope fractionation as a function of bioavailable Fe, the bioavailable Zn concentration was kept constant.

The culture medium we use here is similar to a medium whose history has previously been reviewed by Berges et al. (2001). The seawater base, however, has been adjusted to a final salinity of 35.93 ± 0.01 g $kg^{-1}$ with NaCl. Whereas the concentrations of nitrate, phosphate, and all vitamin supplements follow these authors, silicate was kept at a slightly lower level according to Provasoli (1968). The trace elements manganese (Mn), molybdenum (Mo), and selenium (Se) were also adjusted to the values given by Berges et al. (2001), in contrast to cobalt (Co) whose concentration follows Harrison et al. (1980).

The most important characteristics of the medium for the purposes of this study relate to the concentrations of the metals Fe, Ni, and Zn. Whereas Fe′ was varied in the range between 5.6 and 111.5 pmol $l^{-1}$, the inorganically bound (Me′) and free divalent ($Me^{2+}$) concentrations of the two other metals (Me) have been kept constant. Ni was kept at low levels of 2.33 ± 0.02 and 1.31 ± 0.01 pmol $l^{-1}$ (2 SD, n =18) and Zn at elevated concentrations of 158.8 ± 0.9 and 104.9 ± 0.6 pmol $l^{-1}$ (2 SD, n =18), of Me′ and $Me^{2+}$ respectively. Copper (Cu), which was not present in the previously described recipe, has been added as a hydrated sulfate salt at a final total concentration of 40 nmol $l^{-1}$. This translates to bioavailable Cu′ and $Cu^{2+}$ concentrations as low as ~0.5 and <0.05 pmol $l^{-1}$ (n =18). Aqueous speciation has been calculated according to Sunda et al. (2005) and references therein.

This medium contrasts with that previously used by John et al. (2007) mainly in its Fe concentration, which here was kept several orders of magnitude lower. The rationale for this

modification is further outlined in Section 3.3. The chosen bioavailable Zn level was such that uptake is dominated by the high-affinity pathway (Sunda and Huntsman, 1992), with only a small contribution via low-affinity uptake. The resulting choice of a fairly high Zn concentration, close to where low-affinity uptake also starts to become important, is a compromise between the attempt to avoid a second active mechanism and the necessity to incorporate a minimum Zn quota to allow isotope analysis (see Appendix).

### 3.2 Diatom strains and culturing techniques

Two different diatom strains were obtained from the National Center for Marine Algae and Microbiota (NCMA), formerly known as Provasoli-Guillard Center for Culture of Marine Phytoplankton (CCMP), Bigelow Laboratories, USA. Both strains were obtained and kept axenic by handling them using sterile techniques. These two strains were chosen as both originate in the open ocean oligotrophic surface waters of the Sargasso Sea, North Atlantic. In this study we compare the extensively studied diatom *Thalassiosira oceanica* (CCMP 1005), with a less well-known representative of the genus *Chaetoceros* (CCMP 199).

Light was supplied to phytoplankton cultures in 15- to 9-hour day to night cycles at a constant photon flux density of 40 µmol $m^{-2}$ $s^{-1}$, as mapped with a spherical quantum sensor LI-193 (LI-COR®, Nebraska, USA). All cultures were acclimated to the given light intensity and to low Fe concentrations, for at least 5 transfer cycles. Cell numbers were quantified using light microscopy and a Reichert Bright-Line hemocytometer (Hausser Scientific, USA) with a Neubauer ruling, in which volumes of typically 0.1 µl were counted. Counting results were routinely complemented with Coulter counter cell numbers and volumes. The specific growth rate, µ, was determined by linear regression of the natural logarithm of cell counts in time versus cell number plots. Sterile techniques were used whenever diatom cultures or media solutions were handled. Diatom cells were separated from their residual culturing medium by 0.2 µm membrane filtration, using pre-cleaned vertical twin-membrane centrifugal concentrators (Vivaspin 20, Sartorius, Germany). Media remnants were washed off the collected biomass with UV-treated equatorial Atlantic seawater, with notably low Zn in the range of 0.01-0.05 nmol $kg^{-1}$ (Zhao, 2011).

### 3.3 Fe-hydroxides removal from diatom surfaces

All diatoms cultured in this study were washed only with metal-free equatorial Atlantic seawater. Cultured marine diatoms bear the potential to precipitate Fe-hydroxides on their surface and Zn has a generally high propensity to adsorb onto such Fe-phases. Considering the strong affinity of heavy Zn for Fe-hydroxides (Pokrovsky et al., 2005), their presence could affect the Zn isotope composition of the bulk biomass. Surface treatments that first remove Fe-hydroxides (Tovar-Sanchez et al., 2003) have thus been considered essential to obtain cellular Zn contents or Zn isotope compositions (John et al., 2007). John et al. (2007) speculate that the potential problem of surface Fe-oxides could be avoided by simply lowering the total Fe concentration in the culturing medium Here we briefly summarize arguments in favor of a simple seawater wash.

Much of what is known about intracellular Zn quotas and Zn uptake rates originates from early culturing work consistently conducted by washing cells only with seawater (Sunda and Huntsman, 1992; Ellwood and Hunter, 2000). More recently, it has become possible to image intracellular metal contents and to clearly separate these from surface-associated fractions, through methods such as synchrotron based X-ray fluorescence imaging techniques (Twining et al., 2003). The metal quotas found in early culturing work (*c.f.* Sunda and Huntsman, 1992; Twining et al., 2003) agree well with these found with these in-situ methods, for the same *Thalassiosira* strain, indicating that seawater washes indeed obtain accurate intracellular Zn concentrations.

In previous work, whenever intracellular Fe quotas or Fe uptake rates have been the focus, surface-bound Fe-hydroxides were carefully dissolved (Hudson and Morel, 1989; Sunda and Huntsman, 1995b). The Fe uptake rates obtained in this study, presented later and all attained without any dissolution of solid Fe-phases, are in good agreement with those previously reported (Sunda and Huntsman, 1995b, 1997). We interpret this observation as further evidence for the fact that the total Fe concentrations in the culturing media were sufficiently low to avoid the precipitation of Fe-hydroxides. Six additional cultures per strain were deliberately grown at increased Fe′ levels to yield surface precipitates by design (Table 1).

Tang and Morel (2006) extensively studied the impact of large quantities of surface-bound Fe-hydroxides on the distribution of other transition metals associated with diatom biomass. The P normalized Zn quotas they obtained with NaCl washed diatoms were almost identical, over the entire observed range of Fe-precipitates, with those obtained from experiments in which surface-bound Fe-hydroxides were carefully dissolved. In particular, at low total Fe concentrations, both methods gave identical results. The authors suggest that, under most circumstances, one obtains accurate cellular Zn concentrations just by the removal of media remnants (Tang and Morel, 2006).

John et al. (2007) found that unwashed diatom cells, cultured at the bioavailable Zn concentrations used here, were ~0.6 ‰ heavier than biomass samples from which surface-bound Fe, and possibly co-precipitated Zn, has been removed. These authors also suggest, however, that a simple solution to this problem could be achieved simply by lowering the total Fe concentration, and identified their total medium Fe concentration of 10 μmol $l^{-1}$ as potentially too high to avoid the precipitation of Fe-hydroxides (John and Conway, 2014). If the empirical relationship between total medium Fe concentration and biomass Fe/P ratios (including surface-bound Fe) found by Tang and Morel (2006) for *T. weissflogii* also holds for the *T. oceanica* species cultured by John et al. (2007), then this total medium Fe concentration would imply Fe/P ratios in their biomass >200 mmol $mol^{-1}$. As outlined later, the present study finds mean Fe/P ratios for *T. oceanica* of 1.8 mmol $mol^{-1}$, at least a factor of 100 lower. Hence, we argue that the previously determined impact of surface-bound Fe-hydroxides is not significant for the present study.

### 3.4 Elemental and stable isotope analysis

All biomass samples were re-suspended in pre-cleaned NaCl solutions adjusted to the same osmolality found within diatom cells, to prevent cell lysis. The resulting cell suspensions were pipetted out of the centrifugal concentrator (*c.f.*, previous section) and were dried down before digestion in double distilled 65% $HNO_3$ at 120 °C for 16 hours. All experimental solutions were re-dissolved in 2 % $HNO_3$ for elemental and isotopic analysis, after a final dry-down.

The procedures used for elemental and stable isotope analysis are very similar to those in previous publications from this laboratory (Little et al., 2016; Vance et al., 2016a; Vance et al., 2016b). In brief, a ThermoScientific Element XR$^{TM}$ inductively-coupled plasma mass spectrometer (ICP-MS) was used for elemental analysis, and all isotope analyses were performed on a Neptune Plus$^{TM}$ multiple-collector inductively-coupled plasma mass spectrometer (MC-ICP-MS) of the same manufacturer. Sample purification for isotope analysis was done by anion exchange chromatography (Maréchal et al., 1999; Archer and Vance, 2004; Bermin et al., 2006). Mass fractionation occurring during ion exchange chromatography or associated with the mass spectrometer itself was corrected by using the double-spike approach as described by Bermin et al. (2006) and Zhao et al. (2014), in combination with a data reduction scheme presented by Siebert et al. (2001). The data presented here are given in the standard delta notation, in per mil, reported relative to JMC 3-0749 (Maréchal et al., 1999): $\delta^{66}Zn$ (‰) = [($^{66}Zn/^{64}Zn$)$_{sample}$ / ($^{66}Zn/^{64}Zn$)$_{JMC\ 3\text{-}0749}$] – 1. Accuracy and precision were monitored relative to a secondary standard, IRMM-3702, previously reported to yield a value of +0.32 ‰ (Ponzevera et al., 2006; Cloquet et al., 2008), recently corrected to a value of +0.30 ‰ (Moynier et al., 2017). Relative to JMC-Lyon, we obtain $\delta^{66}Zn$ = 0.30 ± 0.06 ‰ (2 SD, n = 163 over 380 days).

All our culturing results are reported as the fractionation observed between the medium and the separated biomass, here denoted $\Delta^{66}Zn_{biomass\ -\ medium}$ (‰) = $\delta^{66}Zn_{biomass}$ - $\delta^{66}Zn_{medium}$. All diagrams plot the external precision, based on replicate analyses of IRMM-3702 as noted above, except when internal errors on individual samples exceed long-term external reproducibility.

## 4. Results

The new Zn and Fe data presented here (Table 1) allow comparison of two distinct open ocean diatoms, both originating from the same oligotrophic surface waters of the Sargasso Sea, North Atlantic. Whereas *T. oceanica* (Hasle, 1983) has been extensively studied, little is known about the representative of the genus *Chaetoceros* studied here. The mean cellular volume of the two strains was found to be very similar, at 305 µm$^3$ for *T. oceanica* and 315 µm$^3$ for *Chaetoceros*. In contrast to *T. oceanica* cells, the volumes of *Chaetoceros sp.* decrease systematically with

lower medium Fe′, through the range 256 to 350 μm$^3$. This finding conforms with theoretical predictions by Hudson and Morel (1990), suggesting that small cells are favored under Fe-limiting conditions.

### 4.1 Growth suppression due to Fe′ limitation

Both diatom strains reach specific growth rates of about 0.85 d$^{-1}$ at Fe′ concentrations in the range 0.08 to 0.11 nmol l$^{-1}$. Growth is increasingly limited at lower Fe′, but the degree to which this occurs is clearly different for the two species studied. *T. oceanica* is able to maintain a growth rate that is almost half of its initial value (0.41 d$^{-1}$) at a Fe′ level of 0.01 nmol l$^{-1}$. At this Fe′ level *Chaetoceros sp.* suffers growth reduction of 80 %, decreasing to values as low as 0.16 d$^{-1}$ (Figure 2A). Growth suppression has thus been achieved by applying an external forcing, namely Fe′ limitation. Surface area-normalized Fe uptake rates decrease, for both studied species, with decreasing Fe′ concentrations made available to the diatom cell (Figure 2B). All Fe uptake rates reported in this study agree well with those previously reported for Fe′-limited diatom cultures by Sunda and Huntsman (1997).

### 4.2 Zn uptake rates and the distribution of Zn isotopes

Mean biomass associated Zn quotas, here reported for *T. oceanica* and *Chaetoceros sp.*, are in good agreement with those previously obtained for three different *Thalassiosira* strains (Sunda and Huntsman, 1992). The variability in Zn/C, however, is higher than previously reported, spanning a range between 7.4 and 25 μmol mol$^{-1}$ (blue whisker in Figure 3A). It is shown later that this variation in Zn/C is correlated with Fe′ (Table 1).

For *Chaetoceros sp.* surface area normalized Zn uptake rates were found to be in the range of 8.4 to 46.9 nmol m$^{-2}$ d$^{-1}$. Those of *T. oceanica*, in contrast, were higher and consistently exceeded values of 45.2 nmol m$^{-2}$ d$^{-1}$, with the exception of a single aberrant value at 28.9 nmol m$^{-2}$ d$^{-1}$. Moreover, Zn uptake rates of *Chaetoceros sp.* decreased linearly with increasingly suppressed growth. Those of *T. oceanica*, in contrast, decrease with a similar slope from their maximum

313 value to a specific growth rate of ~0.6 $d^{-1}$, after which the slope of growth inhibition becomes
314 steeper (Figure 3B).

315 With respect to the bulk culturing medium, the *T. oceanica* biomass was slightly preferentially
316 enriched in light Zn isotopes, yielding a mean $\Delta^{66}Zn_{\text{biomass - medium}}$ signature of -0.13 ± 0.11 ‰ that
317 is constant across a wide range of generally high Zn uptake rates. The Zn isotope fractionation
318 upon uptake is thus in the same direction as, but smaller than that found by, John et al. (2007), at
319 $\Delta^{66}Zn_{\text{biomass - medium}}$ = -0.41 ± 0.09 ‰, for the same species at similar free Zn levels. It is within
320 uncertainty of that found by John et al. (2007) at free Zn concentrations a factor of 5 lower. In
321 contrast, comparatively low Zn uptake rates obtained with *Chaetoceros sp.* correlate with $\Delta^{66}Zn$
322 $_{\text{biomass - medium}}$ fractionations that range from values as low as -0.42 ± 0.06 ‰ up to +0.85 ± 0.14
323 ‰, the latter at the lowest Zn uptake rates (Figure 3C).

324 **4.3 Physiological interplay between Zn and Fe**

325 The cellular Zn uptake rates of both studied diatom species are correlated with those of Fe, even
326 though the absolute rates of *Chaetoceros sp.* are only about half those of *T. oceanica* (Figure 4).
327 Given that cellular Zn uptake is a function of the specific growth rate (Figure 3B), which is again
328 set by an external forcing, namely Fe′ (Figure 2A), it is valid to also explore Zn uptake
329 dependence on Fe′ (Figure 5).

330 The bioavailable Zn concentration was deliberately kept constant in all experiments, to ensure
331 that Fe′ is the only variable changed in the system. The P-normalized Zn quota was found to be
332 in the range 0.78 to 2.64 mmol $mol^{-1}$ under varied degrees of Fe′ limitation, equivalent to
333 concentrations from 0.01 to 0.11 nmol $l^{-1}$ (Figure 5A). These numbers are in good agreement
334 with previous culturing work reporting cellular Zn quotas, equivalent to Zn/P ratios in the range
335 1 to 2 mmol $mol^{-1}$ (Sunda and Huntsman, 1992, 1995a; reviewed in Twining and Baines, 2013).
336 A few experiments conducted with Fe′ concentrations higher than 0.7 nmol $l^{-1}$, a threshold above
337 which Fe-hydroxides have previously been documented to occur in culturing solutions (Sunda
338 and Huntsman, 1995b, 1997), gave much higher Zn/P ratios, in the range 4.2 to 5.1 and 3.4 to
339 4.2 for *Chaetoceros sp.* and *T. oceanica*, respectively.

Both diatoms show systematically reduced Zn uptake rates with decreasing levels of Fe′ (Figure 5B). The gradient of Zn uptake rates is less steep than those of Fe. *Chaetoceros sp.*, however, whose growth is more severely suppressed relative to that of *T. oceanica*, is also generally characterized by more rapid lowering of Zn uptake rates associated with Fe limitation.

The mean $\Delta^{66}Zn_{\text{biomass - medium}}$ of -0.13 ± 0.11 ‰ for *T. oceanica* is independent of Fe′, similar to the lack of dependence on Zn uptake rates, as described earlier (*c.f.*, Figure 3C). *Chaetoceros sp.*, on the other hand, shows increasingly heavy Zn isotope signatures with decreasing Fe′ concentrations (Figure 5C). The most negative $\Delta^{66}Zn_{\text{biomass - medium}}$ of -0.42 ± 0.04 ‰ observed for *Chaetoceros sp.* were found just below a previously described threshold of 0.7 nmol $l^{-1}$ Fe′, above which Fe-precipitates have been described to occur in diatom cultures (Sunda and Huntsman, 1995b, 1997). Six full replicates of diatom strains cultured above this threshold were found to be more variable and to display more positive $\Delta^{66}Zn_{\text{biomass - medium}}$ than those cultured at the highest Fe′ investigated below this threshold (Figure 5C), consistent with previous findings concerning the impact of surface Fe-hydroxides on Zn isotopes in diatoms (John et al., 2007).

# 5. Discussion

## 5.1 Physiological interplay between Zn and Fe

In the set of experiments reported here an external forcing, namely Fe-limitation, has been applied to suppress diatom growth to a variable extent. The physiological interplay between two intracellularly abundant transition metals can thus be studied. The interest in such an analysis originates in the observation that key diatom habitats in the ocean are often Fe-limited (Martin and Fitzwater, 1988; Boyd et al., 2000), but usually not Zn-limited (Moore et al., 2013). A conceptual understanding of these regimes is thus important.

The approach taken here, for the first time, shows how species dependent differences in the degree to which Fe′ limits growth (Figure 2A) exerts a control on Zn uptake rates (Figure 5B). In contrast to previous work conducted with coastal diatoms (Sunda and Huntsman, 1997), the open marine species studied here exhibit severe growth limitation due to lower Fe′ concentrations

366 (Figure 2A). Sunda and Huntsman (1997) demonstrated that cell surface area normalized Fe
367 uptake rates of all four coastal species they studied can be described with a single saturation
368 equation for nutrient uptake. Described with a kinetic model analogous to that of Michaelis and
369 Menten (1913), the authors found that saturation was reached at a $V_{max}$ of 1276 nmol $m^{-2}$ $d^{-1}$ with
370 a $K_s$ of 0.51 nmol $l^{-1}$. The surface area normalized Fe uptake rates for the oceanic species reported
371 in this contribution can be described with the exact same relationship as for coastal species
372 (Sunda and Huntsman, 1997). We interpret this observation as evidence for the same underlying
373 control *i.e.*, the external forcing from Fe-limitation. On the basis of this finding, the previous
374 relationship can be extended by the two newly characterized oceanic species to yield an updated
375 $V_{max}$ of 1289 ± 263 nmol $m^{-2}$ $d^{-1}$ with a corresponding $K_s$ of 0.53 ± 0.19 nmol $l^{-1}$ (Table 2).

376 The Zn uptake rate is similarly positively dependent on Fe′, though the quantitative nature of that
377 dependency is also somewhat different (see the less steep gradients for the data plotted in Figure
378 5B). There is also apparently a difference between the two organisms studied here. Cause and
379 effect are unclear; it may, for example, be that the more severe suppression of growth in
380 *Chaetoceros* simply reduces the cellular requirement for Zn, a metal that fulfills an important
381 structural function as a cofactor in several essential enzymes (Morel et al., 1994). A prime
382 candidate for an enzyme that might not be needed at reduced growth in the same high quantities
383 as at maximum growth, is the Zn containing carbonic anhydrase (Morel et al., 1994), required
384 for biomass buildup by fixation of atmospheric $CO_2$.

385 The general distribution of Zn isotopes exhibits features as a function of Fe′ (Figure 5C) that are
386 analogous to those found for Zn uptake rates (Figure 3C). Whereas *T. oceanica* again shows little
387 variability around a mean $\Delta^{66}Zn_{\text{biomass - medium}}$ of -0.13 ± 0.11 ‰, *Chaetoceros* cells were found to
388 be increasingly heavy with decreasing Fe′ concentrations (Figure 5C). In this context it is
389 important to note again that all these cultures have only been washed with metal-free equatorial
390 Atlantic seawater. To avoid the problem of surface bound Fe hydroxides, the media used here
391 were adjusted to extremely low total Fe concentrations (*c.f.*, Section 3.3). The stronger affinity
392 of heavy Zn for solid Fe-hydroxides (Pokrovsky et al., 2005) would be expected to cause the

biomass to be increasingly more fractionated in $\Delta^{66}Zn$ with increasing quantities of surface bound Fe phases. Contrary to this expectation, the most negative signatures of -0.42 ± 0.04 ‰ were observed at the highest Fe′, with increasing $\Delta^{66}Zn_{\text{biomass - medium}}$ values progressively further away from a previously described threshold of 0.7 nmol $l^{-1}$, above which Fe-precipitates have been documented to occur in diatom cultures (vertical dashed line in Figure 5; Sunda and Huntsman, 1995b, 1997). We tested for the impact of Fe-hydroxides with six full culturing replicates of both strains above the threshold of precipitation, and found the results to be variable. The most negative $\Delta^{66}Zn_{\text{biomass - medium}}$ were in good agreement with the numbers observed just below the threshold. Consistent with Pokrovsky et al. (2005), the heaviest fractionation were found to be +0.18 to 0.28 ‰ heavier than the most negative (Figure 5C).

### 5.2 Cellular Zn quotas and Zn/P ratios at low Fe′

The Monod (1949) and Michaelis and Menten (1913) equations are mathematical models that describe phytoplankton growth (Monod) and nutrient uptake (Michaelis-Menten) rates. Both equations, identical in their general form, relate growth rate ($\mu$) and nutrient uptake rate ($\upsilon$) to the nutrient concentration available in an aqueous environment surrounding the cell. In both descriptions, maximum growth ($\mu_{max}$) or saturation of uptake ($V_{max}$) is reached at high ambient concentrations of a potentially limiting resource, in this case Fe′. The rate of increase in growth or uptake below $\mu_{max}$ and $V_{max}$ are conventionally described in terms of empirical half-growth (k) and half-saturation ($K_S$) constants, defined as the limiting nutrient concentrations at which $\mu/\mu_{max}$ and $\upsilon/V_{max}$ equals 0.5 (see Figure 6).

The Droop (1973) equation ($\upsilon = \mu Q$) contrasts with the above approaches in that it is the intracellular nutrient quota (Q) that is used to relate growth ($\mu$) and nutrient uptake ($\upsilon$) rates. This treatment accounts for the fact that any organism, even at infinitely low growth rates, will have an internal nutrient quota that is significantly larger than zero. The lower the ambient substrate concentrations, the more the cellular nutrient quota is likely to deviate from what would be expected if the latter is tied only to biomass build-up. In the following we use the Droop

419 relationship to explore the cellular Zn quotas for known growth and metal uptake kinetics (Figure
420 6), in order to understand their variability at progressively lower ambient Fe′-levels.

421 The specific growth rate of *T. oceanica* and *Chaetoceros sp.*, described after Monod (1949) as a
422 function of bioavailable Fe′, yield maxima ($\mu_{max}$) of 0.99 ± 0.08 $d^{-1}$ and 0.96 ± 0.07 $d^{-1}$ with half
423 saturation constants of 0.021 ± 0.004 nmol $l^{-1}$ and 0.009 ± 0.004 nmol $l^{-1}$, respectively (Table 2,
424 Figure 6A). A similarly quantitative description of Zn uptake rates was obtained with a pseudo-
425 Michaelis-Menten kinetics (Figure 6B). With the prefix 'pseudo' it is emphasized that the Zn
426 uptake rate is not expressed as a function of the bioavailable Zn concentration as is
427 conventionally done (Michaelis and Menten, 1913), but instead as a function of Fe′. The
428 justification for doing so originates in the results described earlier, showing that Zn uptake rates
429 are coupled to those of Fe (Figure 4), with both dependent on the concentration of Fe′ available
430 in the medium (Figure 2B). It is important to note that the set of parameters obtained, *i.e.* a $V_{max}$
431 of 58.9 ± 8.6 nmol $m^{-2}$ $d^{-1}$ and 91.9 ± 2.2 nmol $m^{-2}$ $d^{-1}$ with half saturation constants of 0.038 ±
432 0.013 nmol $l^{-1}$ and 0.005 ± 0.001 nmol $l^{-1}$ Fe′, for *T. oceanica* and *Chaetoceros sp.*, respectively
433 (Table 2), are not universally valid. Instead, these numbers are specific to a Fe-limitation scenario
434 at the given bioavailable Zn concentration.

435 The intracellular Zn quota has been suggested to be linked to its uptake rate divided by the
436 specific growth rate of the organism (Droop, 1973). With the aid of the Droop equation and our
437 quantitative descriptions of specific growth rate and Zn uptake as a function of Fe′, the cellular
438 Zn quota is seen to change most significantly under Fe limiting conditions (Figure 6C). Cellular
439 Zn quotas can be calculated to decrease by 38 % for the severely Fe limited *Chaetoceros sp.*,
440 while *T. oceanica* cells experience a much smaller change, with Zn increasing by 7.6 % at the
441 lowest Fe′.

442 Droop quotas can furthermore help to elucidate the physiological peculiarities of the two distinct
443 diatom strains when exposed to identical environmental constraints. *T. oceanica* can sustain high
444 reproduction rates, even if Fe gets to low concentrations, and must contain an effective resource-
445 acquisition machinery to ensure consistently high cellular Zn quotas. *Chaetoceros sp.*, in contrast,

446 is best adapted for exponential growth in Fe-rich waters, but suffers from low Fe′ concentrations,
447 at levels that do not affect *T. oceanica*. In contrast to *T. oceanica*, the growth rates of *Chaetoceros*
448 *sp.* are considerably lower at reduced Fe′ levels. A lower expression of growth-related enzymes
449 is required to sustain the observed reproduction rates. In other words, at high Fe′, *Chaetoceros*
450 holds a high proportion of growth machinery, significantly reduced when growth becomes
451 limited.

452 **5.3 Zn uptake rates and Zn isotope fractionation upon uptake**

453 The new Zn stable isotope data presented here have two principal features. Firstly, a species
454 whose growth is less affected by low Fe′, *T. oceanica* (Figure 2A), is able to maintain relatively
455 high Zn uptake rates (Figure 3B), with a nearly constant and slightly negative (-0.02 to
456 -0.19 ‰) fractionation of $\Delta^{66}Zn_{\text{biomass - medium}}$ (Figure 3C). Secondly, the species whose growth is
457 severely Fe-limited, the representative of the genus *Chaetoceros* studied here, shows more
458 variable biomass Zn isotope signatures at a generally low Zn uptake rate (Figure 3B and C). For
459 Zn uptake rates at the higher end of the range for *Chaetoceros*, those that overlap with those of
460 *T. oceanica*, *Chaetoceros* also shows small negative $\Delta^{66}Zn_{\text{biomass - medium}}$. But at the lower uptake
461 rates that occur at low Fe′, it records variably positive $\Delta^{66}Zn_{\text{biomass - medium}}$, up to +0.85 ‰.

462 With regard to the first of these observations, it is theoretically possible that that faster diffusion
463 of light isotopes (Rodushkin et al., 2004) through the medium could contribute to the enrichment
464 of light Zn isotopes within the phytoplankton cell, but in none of these experiments would
465 transport to the cell have been diffusion limited. In fact, the constant and slightly negative
466 fractionation for *T. oceanica* is consistent with negligible fractionation upon uptake, given the
467 presence of EDTA as a transition metal buffer in the culturing medium. Previous experiments
468 studying the equilibrium fractionation between chelating resins and free Zn found heavy Zn
469 isotopes preferentially associated with this ligand. The corresponding enrichment of light
470 isotopes in the non-chelated Zn pool is consequently in the range of -0.16 to -0.33 ‰ (Ban et al.,
471 2002; Ding et al., 2010a; Ding et al., 2010b; Markovic et al., 2017). As it is the free divalent
472 metal that is bioavailable (Anderson et al., 1978; Anderson and Morel, 1982; Hudson, 1998),

diatom extract Zn from a pool that is significantly lighter than an equilibrated bulk medium, used as a reference to calculate the fractionation upon uptake into cells. A biomass sample such as *T. oceanica*, here consistently found to show fractionations ($\Delta^{66}Zn_{\text{biomass - medium}}$) of around -0.13 ‰, might consequently only reflect the aqueous equilibrium between the bioavailable free Zn and EDTA in the culturing medium, potentially implying no fractionation at all associated with Zn uptake, an interpretation that has previously been put forward for similar culturing results by John et al. (2007).

*A priori*, the second observation could be explained in two different, though perhaps related, ways. One possible explanation of the heavy isotope signatures seen in *Chaetoceros sp.* at low Zn uptake rates could relate to the more severe growth limitation seen for this species at low Fe′. Previous researchers have shown that molecules such as saccharides can enhance the bioavailability of Fe to marine phytoplankton (Hassler et al., 2011), including diatoms belonging to the genus *Chaetoceros* (Hassler et al., 2011; Raposo et al., 2013). The release of surface-bound organics is a survival strategy to scavenge Fe, which progressively becomes scarcer under the environmental conditions studied here. Such saccharides almost certainly scavenge heavy Zn (Coutaud et al., 2014). Thus, increasing amounts of such extracellular polymeric substances (EPS) excreted with decreasing Fe′ might represent a possible explanation for the observed heavy Zn isotope signatures. Alternatively, Zn associated with EPS could simply have greater relative importance at the decreased quantities of Zn that are internalized at low Fe′. We are not aware of any published work on EPS associated with *T. oceanica*, but this does not mean that the diatom is unable to exude such components. Whether EPS could cause such heavy $\Delta^{66}Zn_{\text{biomass - medium}}$ is highly speculative at this stage and awaits further investigation, ideally directly comparing the two diatom strains.

The second possible explanation is a switch from a kinetic control of Zn uptake at high uptake rates to an equilibrium control as uptake rate declines. In the following, the term ‘kinetic isotope effect’ refers to all those effects that cause the fractionation of stable Zn isotopes associated with incomplete and unidirectional processes, such as those typical for dissociation or biologically

500 mediated chemical reactions. There is a distinct threshold in the variation of biomass Zn isotope
501 signatures as a function of Zn uptake rate, with $\Delta^{66}Zn_{\text{biomass - medium}}$ increasing sharply at a surface
502 area normalized uptake rate below 35 ± 10 nmol $m^{-2}$ $d^{-1}$. If the dehydration of the hexa-aquo Zn
503 to form an inner-sphere surface complex at the transporter site (Figure 1) is the rate limiting step
504 in the uptake kinetics (Hudson and Morel, 1990; Hudson, 1998; Sunda and Huntsman, 1998),
505 light isotopes would undergo this transformation slightly faster than heavy Zn (Bigeleisen and
506 Wolfsberg, 1958; and references therein). Zn uptake may be entirely under kinetic control above
507 this threshold (Figure 7A), a situation in which every transport enzyme runs at its maximum
508 turnover. This is supported by the fact that once the observed maximum preference for light
509 isotopes is achieved, it remains constant. The cell can still increase the number of enzymes per
510 unit area of cell wall to further facilitate higher Zn uptake rates, but the dehydration at individual
511 transporter sites would remain constant, and governs the maximum achievable preference for
512 lighter Zn isotopes (Figure 7B).

513 If the cellular Zn uptake rate is down-regulated to values lower than the dehydration rate of the
514 Zn hexa-aquo complex, the kinetically controlled preference for light isotopes at the transporter
515 site would become progressively less dominant (Figure 7C). In our experiments, the observed
516 fractionation ($\Delta^{66}Zn_{\text{biomass - medium}}$) becomes increasingly positive with lower Zn uptake rates.
517 Given the strength of bonds between Zn and many organic ligands, isotopically heavier biomass
518 signatures at low uptake rates are consistent with an increasing equilibrium component
519 (Bigeleisen and Mayer, 1947; Schauble, 2004; Fujii et al., 2014), and this has been observed
520 experimentally for Zn (Jouvin et al., 2009). It is currently not entirely clear whether Zn uptake
521 can be low enough that conditions close to thermodynamic equilibrium start to become relevant.
522 The sharp increase in $\Delta^{66}Zn_{\text{biomass - medium}}$ is thus interpreted as a continuum that is likely to develop
523 towards equilibrium, but in any case away from a purely kinetically controlled system.

524 One could postulate that the data in Figure 3C represent a single relationship for both species. In
525 this case, and consistent with the above explanation of heavy versus light Zn isotopes, it is Zn
526 uptake rate itself that is the key controlling variable for biomass Zn isotope signatures. In this

view, *T. oceanica* never shows heavy isotope signatures because it exhibits Zn uptake rates that are mostly higher than the threshold around 35 nmol $m^{-2}$ $d^{-1}$, even at the lowest Fe′. Alternatively, both diatoms might follow their individual pattern. In this view, however, *Chaetoceros sp.* never reaches Zn uptake rates high enough to achieve a constant preference for light isotopes. Even though this view is currently only poorly supported by the available data, this would imply species-dependent differences in the maximum preference for light Zn isotopes. Such an observation, in consequence, suggests structural differences in the active site of the transporter proteins or two different uptake mechanisms.

# 6. Concluding remarks: implications for oceanic Zn isotopes

An important finding of the experiments documented here is that the extent to which growth is limited by an external forcing, such as Fe′, controls the pace of Zn uptake (Figure 7D). If reduced Zn uptake is a physiological response to lower cellular Zn demands, it seems likely that other external forcings might cause a similar down-regulation of the Zn uptake rate, as an indirect consequence of growth suppression.

These results potentially have important implications for the interpretation of the global oceanic distribution of Zn and its isotopes, though there are also open questions that require further experimentation. In terms of the global surface ocean, the Southern Ocean has already been noted to be unusual. Here diatoms dominate Zn cycling (Vance et al., 2017), and the lack of Zn isotope fractionation in the dissolved pool across a 40-fold drop in concentration as diatoms deplete it (Wyatt et al., 2014; Zhao et al., 2014; Vance et al., 2017) suggests a lack of fractionation upon uptake. The fact that this lack of isotope fractionation occurs in a region with severe Fe limitation is, at first sight, somewhat at odds with the experimental findings here. On the other hand, where Fe is supplied to the Southern Ocean, diatoms grow extremely rapidly, in blooms (Boyd et al., 2000). Another key feature of the Southern Ocean is that it is the only known surface ocean location where total Zn concentrations far outstrip those of the complexing organic ligands, leading to very high bioavailable free Zn ions (Baars and Croot, 2011). This has two impacts. First, Zn uptake rates will be rapid in response, both to high bioavailable Zn (this study, Sunda

554 and Huntsman, 1992) and to a diatom ecology that is characterized by fast growing blooms in
555 the Southern Ocean. Second, if a substantial portion of the total Zn pool is represented by free
556 Zn, then the isotopic composition of the latter pool will be close to the bulk dissolved pool itself.
557 In this case, the lack of fractionation during uptake may simply suggest that Zn uptake is under
558 kinetic control.

559 Much of the low latitude upper Atlantic Ocean appears to exhibit light Zn isotope compositions
560 in the dissolved pool (Conway and John, 2014a). Zhao et al. (2011; 2014) suggest that light sub-
561 surface Zn isotopes might be driven by very shallow regeneration of a light cellular signature
562 created in the photic zone immediately above. In terms of the experimental data presented here,
563 the light biomass signature could derive from a very small free Zn pool, which outside the
564 Southern Ocean is tiny relative to the organically complexed pool and must be isotopically light
565 relative to the total dissolved reservoir (Ban et al., 2002; Jouvin et al., 2009; Ding et al., 2010a;
566 Ding et al., 2010b; Markovic et al., 2017), again without fractionation upon uptake. John and
567 Conway (2014), on the other hand, favor scavenging of heavy isotopes onto organic matter,
568 creating an isotopically light residual pool, as a possible explanation for a light upper ocean. It is
569 also interesting that the most severely Fe-limited *Chaetoceros* cultures, with the lowest Zn uptake
570 rates, show the heaviest Zn isotope signatures. The findings here allow consideration of another
571 potential driver: residual light signatures in the surface ocean could be driven by preferential
572 uptake of the heavy isotope at very slow rates of Zn uptake.

573 # Appendix

574 The data re-evaluated in this appendix originates in Sunda and Huntsman (1992). The previous
575 dataset was re-evaluated to more precisely identify the highest bioavailable $Zn^{2+}$ concentration
576 that is still likely to be explained by a single, high-affinity, uptake mechanism alone (Figure A.1),
577 which is important for the experiments in this paper because we needed to identify the highest
578 $Zn^{2+}$ concentration that could be used without introducing the further complication of two uptake
579 mechanisms.

This question was addressed by assuming that high-affinity uptake can be described by the Michaelis-Menten equation. Furthermore, it was assumed that any additionally active mechanism, that is able to further increase uptake above the maximum of high-affinity uptake, would negatively impact a Michaelis-Menten curve fit. The previously reported dataset was incrementally explored by changing the number of samples in the evaluation scheme (Figure A.2). Zn/C ratios recorded at the lowest $Zn^{2+}$ concentrations were always included in the calculated curve fits. Ratios obtained at the highest $Zn^{2+}$ were incrementally taken out of the analysis. Datasets from the minimum up to $Zn^{2+}$ concentrations of ~100, 10, 1, 0.3, and 0.1 nmol $l^{-1}$ were evaluated in the given order. The root mean squared error (RMSE) of the Michaelis-Menten equation has been used as the evaluation criterion to assess the goodness of fit. The dataset was assumed to be adequately described by the Michaelis-Menten fit corresponding to a single, high-affinity, uptake mechanism when the root mean squared error (RMSE) falls below a numerical value of 10, here considered a reliable measure for the accuracy of the fit (Supplementary Figure 2C and D). More conservative estimates would set a RMSE threshold of 7.5 (Supplementary Figure 2E and F). The following root mean squared errors were achieved for the above listed $Zn^{2+}$ concentrations: 630.4, 17.2, 10.94, 7.75, and 6.49 (Supplementary Figure 2). On the basis of this analysis $Zn^{2+}$ concentrations up to 0.1 nmol $l^{-1}$, perhaps up to 0.3 nmol $l^{-1}$, can be explained with a single Zn uptake mechanism. Up to this concentration, uptake is likely to be dominated by high-affinity pathways with only a marginal contribution of an additionally active low-affinity pathway. Given this result, a $Zn^{2+}$ concentration of 0.1 nmol $l^{-1}$ was used here.

## Acknowledgements

We are grateful to Alysia D. Cox for help with setting up a phytoplankton culturing lab at ETH Zurich and to Timothy I. Eglinton for allowing us access to biology laboratories and incubator facilities. We also wish to thank Corey Archer for valuable support with elemental and isotopic analysis and Amélie Ritscher for her work as a research assistant at ETH Zurich. Finally we thank Susan Little for constructive feedback on a previous manuscript of this paper, Laura Wasylenki and an anonymous reviewer for constructive reviews, and Claudine Stirling for efficient editorial

handling. Financial support was provided by ETH and the Swiss National Science Foundation (SNF) through grant 200021-143262.

## References

Abouchami, W., Galer, S.J.G., de Baar, H.J.W., Alderkamp, A.C., Middag, R., Laan, P., Feldmann, H. and Andreae, M.O. (2011) Modulation of the Southern Ocean cadmium isotope signature by ocean circulation and primary productivity. Earth and Planetary Science Letters 305, 83-91.

Anderson, M. and Morel, F. (1982) The influence of aqueous iron chemistry on the uptake of iron by the coastal diatom *Thalassiosira weissflogii*. Limnology and Oceanography 27, 789-813.

Anderson, M.A., Morel, F.M.M. and Guillard, R.R.L. (1978) Growth limitation of a coastal diatom by low zinc ion activity. Nature 276, 70-71.

Archer, C. and Vance, D. (2004) Mass discrimination correction in multiple-collector plasma source mass spectrometry: an example using Cu and Zn isotopes. Journal of Analytical Atomic Spectrometry 19, 656-665.

Archer, C., Vance, D. and Lohan, M. (2016) Zinc and nickel isotope systematics in the South Atlantic Ocean, Goldschmidt conference abstract, Yokohama, Japan, p. 97.

Armbrust, E.V. (2009) The life of diatoms in the world's oceans. Nature 459, 185-192.

Armbrust, E.V., Berges, J.A., Bowler, C., Green, B.R., Martinez, D., Putnam, N.H., Zhou, S., Allen, A.E., Apt, K.E., Bechner, M., Brzezinski, M.A., Chaal, B.K., Chiovitti, A., Davis, A.K., Demarest, M.S., Detter, J.C., Glavina, T., Goodstein, D., Hadi, M.Z., Hellsten, U., Hildebrand, M., Jenkins, B.D., Jurka, J., Kapitonov, V.V., Kröger, N., Lau, W.W.Y., Lane, T.W., Larimer, F.W., Lippmeier, J.C., Lucas, S., Medina, M., Montsant, A., Obornik, M., Parker, M.S., Palenik, B., Pazour, G.J., Richardson, P.M., Rynearson, T.A., Saito, M.A., Schwartz, D.C., Thamatrakoln, K., Valentin, K., Vardi, A., Wilkerson, F.P. and Rokhsar, D.S. (2004) The genome of the diatom *Thalassiosira pseudonana*: ecology, evolution, and metabolism. Science 306, 79-86.

Baars, O. and Croot, P.L. (2011) The speciation of dissolved zinc in the Atlantic sector of the Southern Ocean. Deep Sea Research Part II: Topical Studies in Oceanography 58, 2720-2732.

Ban, Y., Aida, M., Nomura, M. and Fujii, Y. (2002) Zinc isotope separation by ligand exchange chromatography using cation exchange resin. Journal of Ion Exchange 13, 46-52.

Berges, J.A., Franklin, D.J. and Harrison, P.J. (2001) Evolution of an artificial seawater medium: improvements in enriched seawater, artificial water over the last two decades. Journal of Phycology 37, 1138-1145.

Bermin, J., Vance, D., Archer, C. and Statham, P.J. (2006) The determination of the isotopic composition of Cu and Zn in seawater. Chemical Geology 226, 280-297.

Bigeleisen, J. and Mayer, M.G. (1947) Calculation of equilibrium constants for isotopic exchange reactions. The Journal of Chemical Physics 15, 261-267.

Bigeleisen, J. and Wolfsberg, M. (1958) Theoretical and experimental aspects of isotope effects in chemical kinetics. Advances in Chemical Physics, 15-76.

Boyd, P.W. and Ellwood, M.J. (2010) The biogeochemical cycle of iron in the ocean. Nature Geoscience 3, 675-682.

Boyd, P.W., Watson, A.J., Law, C.S., Abraham, E.R., Trull, T., Murdoch, R., Bakker, D.C.E., Bowie, A.R., Buesseler, K.O., Chang, H., Charette, M., Croot, P., Downing, K., Frew, R., Gall, M., Hadfield, M., Hall, J., Harvey, M., Jameson, G., LaRoche, J., Liddicoat, M., Ling, R., Maldonado, M.T., McKay, R.M., Nodder, S., Pickmere, S., Pridmore, R., Rintoul, S., Safi, K., Sutton, P., Strzepek, R., Tanneberger, K., Turner, S., Waite, A. and Zeldis, J. (2000) A mesoscale phytoplankton bloom in the polar Southern Ocean stimulated by iron fertilization. Nature 407, 695-702.

Bruland, K.W. (1980) Oceanographic distributions of cadmium, zinc, nickel, and copper in the North Pacific Earth and Planetary Science Letters 47, 176-198.

Bruland, K.W. (1989) Complexation of zinc by natural organic ligands in the central North Pacific. Limnology and Oceanography 34, 269-285.

Cloquet, C., Carignan, J., Lehmann, M. and Vanhaecke, F. (2008) Variation in the isotopic composition of zinc in the natural environment and the use of zinc isotopes in biogeosciences: a review. Analytical and Bioanalytical Chemistry 390, 451-463.

Conway, T.M. and John, S.G. (2014a) The biogeochemical cycling of zinc and zinc isotopes in the North Atlantic Ocean. Global Biogeochemical Cycles 28, 1111-1128.

Conway, T.M. and John, S.G. (2014b) Quantification of dissolved iron sources to the North Atlantic Ocean. Nature 511, 212-215.

Conway, T.M. and John, S.G. (2015a) Biogeochemical cycling of cadmium isotopes along a high-resolution section through the North Atlantic Ocean. Geochimica et Cosmochimica Acta 148, 269-283.

Conway, T.M. and John, S.G. (2015b) The cycling of iron, zinc and cadmium in the North East Pacific Ocean – insights from stable isotopes. Geochimica et Cosmochimica Acta 164, 262-283.

Coutaud, A., Meheut, M., Viers, J., Rols, J.-L. and Pokrovsky, O.S. (2014) Zn isotope fractionation during interaction with phototrophic biofilm. Chemical Geology 390, 46-60.

Crawford, D.W., Lipsen, M.S., Purdie, D.A., Lohan, M.C., Statham, P.J., Whitney, F.A., Putland, J.N., Johnson, W.K., Sutherland, N., Peterson, T.D., Harrison, P.J. and Wong, C.S. (2003) Influence of zinc and iron enrichments on phytoplankton growth in the Northeastern Subarctic Pacific. Limnology and Oceanography 48, 1583-1600.

Ding, X., Nomura, M. and Fujii, Y. (2010a) Zinc isotope effects by chromatographic chelating exchange resin. Progress in Nuclear Energy 52, 164-167.

Ding, X., Nomura, M., Suzuki, T. and Fujii, Y. (2010b) Chromatographic zinc isotope separation by chelating exchange resin. Chromatographia 71, 195-199.

Donat, J.R. and Bruland, K.W. (1990) A comparison of two voltammetric techniques for determining zinc speciation in Northeast Pacific Ocean waters. Marine Chemistry 28, 301-323.

Droop, M.R. (1973) Some thoughts on nutrient limitation in algae. Journal of Phycology 9, 264-272.

Ellwood, M.J. (2004) Zinc and cadmium speciation in subantarctic waters east of New Zealand. Marine Chemistry 87, 37-58.

Ellwood, M.J. and Hunter, K.A. (2000) The incorporation of zinc and iron into the frustule of the marine diatom *Thalassiosira pseudonana*. Limnology and Oceanography 45, 1517–1524.

Ellwood, M.J. and Van den Berg, C.M.G. (2000) Zinc speciation in the Northeastern Atlantic Ocean. Marine Chemistry 68, 295-306.

Fujii, T., Moynier, F., Blichert-Toft, J. and Albarède, F. (2014) Density functional theory estimation of isotope fractionation of Fe, Ni, Cu, and Zn among species relevant to geochemical and biological environments. Geochimica et Cosmochimica Acta 140, 553-576.

Harrison, P.J., Waters, R.E. and Taylor, F.J.R. (1980) A broad spectrum artificial sea water medium for coastal and open ocen phytoplankton. Journal of Phycology 16, 28-35.

Hasle, G.R. (1983) The marine, planktonic diatoms *Thalassiosira oceanica* sp. nov. and *T. partheneia*. Journal of Phycology 19, 220-229.

Hassler, C.S., Schoemann, V., Nichols, C.M., Butler, E.C.V. and Boyd, P.W. (2011) Saccharides enhance iron bioavailability to Southern Ocean phytoplankton. Proceedings of the National Academy of Sciences 108, 1076-1081.

Hudson, R.J.M. (1998) Which aqueous species control the rates of trace metal uptake by aquatic biota? Observations and predictions of non-equilibrium effects. Science of The Total Environment 219, 95-115.

Hudson, R.J.M. and Morel, F.M.M. (1989) Distinguishing between extra- and intracellular iron in marine phytoplankton. Limnology and Oceanography 34, 1113-1120.

Hudson, R.J.M. and Morel, F.M.M. (1990) lron transport in marine phytoplankton: kinetics of cellular and medium coordination reactions. Limnology and Oceanography 35, 1002-1020.

John, S.G. and Conway, T.M. (2014) A role for scavenging in the marine biogeochemical cycling of zinc and zinc isotopes. Earth and Planetary Science Letters 394, 159-167.

John, S.G., Geis, R.W., Saito, M.A. and Boyle, E.A. (2007) Zinc isotope fractionation during high-affinity and low-affinity zinc transport by the marine diatom *Thalassiosira oceanica*. Limnology and Oceanography 52, 2710-2714.

Jouvin, D., Louvat, P., Juillot, F., Maréchal, C.N. and Benedetti, M.F. (2009) Zinc isotopic fractionation: why organic matters. Environmental Science & Technology 43, 5747-5754.

Lis, H., Shaked, Y., Kranzler, C., Keren, N. and Morel, F.M.M. (2015) Iron bioavailability to phytoplankton: an empirical approach. International Society for Microbial Ecology Journal 9, 1003-1013.

Little, S.H., Vance, D., McManus, J. and Severmann, S. (2016) Key role of continental margin sediments in the oceanic mass balance of Zn and Zn isotopes. Geology 44, 207-210.

Little, S.H., Vance, D., Walker-Brown, C. and Landing, W.M. (2014) The oceanic mass balance of copper and zinc isotopes, investigated by analysis of their inputs, and outputs to ferromanganese oxide sediments. Geochimica et Cosmochimica Acta 125, 673-693.

Lohan, M.C., Crawford, D.W., Purdie, D.A. and Statham, P.J. (2005) Iron and zinc enrichments in the northeastern subarctic Pacific: ligand production and zinc availability in response to phytoplankton growth. Limnology and Oceanography 50, 1427-1437.

Maréchal, C.N., Télouk, P. and Albarède, F. (1999) Precise analysis of copper and zinc isotopic compositions by plasma-source mass spectrometry. Chemical Geology 156, 251-273.

Markovic, T., Manzoor, S., Humphreys-Williams, E., Kirk, G., Vilar, R. and Weiss, D.J. (2017) Experimental determination of zinc isotope fractionation in complexes with the phytosiderophore 2'-deoxymugeneic acid (DMA) and its structural analogues, and implications for plant uptake mechanisms. Environmental Science & Technology 51, 98–107.

Martin, J.H. and Fitzwater, S.E. (1988) Iron deficiency limits phytoplankton growth in the north-east Pacific subarctic. Nature 331, 341-343.

Martin, J.H., Gordon, R.M., Fitzwater, S. and Broenkow, W.W. (1989) VERTEX: phytoplankton/iron studies in the Gulf of Alaska. Deep Sea Research Part A. Oceanographic Research Papers 36, 649-680.

Michaelis, L. and Menten, M.L. (1913) Die Kinetik der Invertinwirkung Biochemische Zeitschrift 49, 333–369.

Monod, J. (1949) The Growth of Bacterial Cultures. Annual Review of Microbiology 3, 371-394.

Moore, C.M., Mills, M.M., Arrigo, K.R., Berman-Frank, I., Bopp, L., Boyd, P.W., Galbraith, E.D., Geider, R.J., Guieu, C., Jaccard, S.L., Jickells, T.D., La Roche, J., Lenton, T.M., Mahowald, N.M., Maranon, E., Marinov, I., Moore, J.K., Nakatsuka, T., Oschlies, A., Saito, M.A., Thingstad, T.F., Tsuda, A. and Ulloa, O. (2013) Processes and patterns of oceanic nutrient limitation. Nature Geoscience 6, 701-710.

797 Morel, F.M.M., Milligan, A.J. and Saito, M.A. (2003) Marine bioinorganic chemistry: the role
798 of trace metals in the oceanic cycles of major nutrients, in: Heinrich, D.H., Karl, K.T. (Eds.),
799 Treatise on Geochemistry. Pergamon, Oxford, pp. 113-143.
800
801 Morel, F.M.M., Reinfelder, J.R., Roberts, S.B., Chamberlain, C.P., Lee, J.G. and Yee, D. (1994)
802 Zinc and carbon co-limitation of marine phytoplankton. Nature 369, 740-742.
803
804 Morel, F.M.M., Rueter, J.G., Anderson, D.M. and Guillard, R.R.L. (1979) AQUIL: a chemically
805 defined phytoplankton culture medium for trace metal studies. Journal of Phycology 15, 135-
806 141.
807
808 Moynier, F., Vance, D., Fujii, T. and Savage, P. (2017) The isotope geochemistry of zinc and
809 copper, Non-traditional stable isotopes. Mineralogical Society of America, pp. 543-600.
810
811 Pokrovsky, O.S., Viers, J. and Freydier, R. (2005) Zinc stable isotope fractionation during its
812 adsorption on oxides and hydroxides. Journal of Colloid and Interface Science 291, 192-200.
813
814 Ponzevera, E., Quétel, C.R., Berglund, M., Taylor, P.D.P., Evans, P., Loss, R.D. and Fortunato,
815 G. (2006) Mass discrimination during MC-ICPMS isotopic ratio measurements: investigation by
816 means of synthetic isotopic mixtures (IRMM-007 series) and application to the calibration of
817 natural-like zinc materials (Including IRMM-3702 and IRMM-651). Journal of the American
818 Society for Mass Spectrometry 17, 1413-1428.
819
820 Provasoli, L. (1968) Media and prospects for the cultivation of marine algae, Cultures and
821 Collections of Algae. Proceedings of the US-Japan Conference, Hakone. Japanese Society for
822 Plant Physiology, Hakone, Japan, pp. 63-75.
823
824 Raposo, M., de Morais, R. and Bernardo de Morais, A. (2013) Bioactivity and Applications of
825 Sulphated Polysaccharides from Marine Microalgae. Marine drugs 11, 233.
826
827 Rodushkin, I., Stenberg, A., Andrén, H., Malinovsky, D. and Baxter, D.C. (2004) Isotopic
828 fractionation during diffusion of transition metal ions in solution. Analytical Chemistry 76, 2148-
829 2151.
830
831 Schauble, E.A. (2004) Applying stable isotope fractionation theory to new systems. Reviews in
832 Mineralogy and Geochemistry 55, 65-111.
833
834 Shaked, Y., Kustka, A.B. and Morel, F.M.M. (2005) A general kinetic model for iron acquisition
835 by eukaryotic phytoplankton. Limnology and Oceanography 50, 872-882.
836
837 Shaked, Y. and Lis, H. (2012) Disassembling iron availability to phytoplankton. Frontiers in
838 Microbiology 3, 1-26.
839
840 Siebert, C., Nägler, T.F. and Kramers, J.D. (2001) Determination of molybdenum isotope
841 fractionation by double-spike multicollector inductively coupled plasma mass spectrometry.
842 Geochemistry, Geophysics, Geosystems 2, 1032.
843
844 Smetacek, V., Klaas, C., Strass, V.H., Assmy, P., Montresor, M., Cisewski, B., Savoye, N.,
845 Webb, A., d'Ovidio, F., Arrieta, J.M., Bathmann, U., Bellerby, R., Berg, G.M., Croot, P.,

Gonzalez, S., Henjes, J., Herndl, G.J., Hoffmann, L.J., Leach, H., Losch, M., Mills, M.M., Neill, C., Peeken, I., Rottgers, R., Sachs, O., Sauter, E., Schmidt, M.M., Schwarz, J., Terbruggen, A. and Wolf-Gladrow, D. (2012) Deep carbon export from a Southern Ocean iron-fertilized diatom bloom. Nature 487, 313-319.

Sunda, W. and Huntsman, S. (2003) Effect of pH, light, and temperature on Fe–EDTA chelation and Fe hydrolysis in seawater. Marine Chemistry 84, 35-47.

Sunda, W.G. and Huntsman, S.A. (1992) Feedback interactions between zinc and phytoplankton in seawater. Limnology and Oceanography 37, 25-40.

Sunda, W.G. and Huntsman, S.A. (1995a) Cobalt and zinc interreplacement in marine phytoplankton: biological and geochemical implications. Limnology and Oceanography 40, 1404-1417.

Sunda, W.G. and Huntsman, S.A. (1995b) Iron uptake and growth limitation in oceanic and coastal phytoplankton. Marine Chemistry 50, 189-206.

Sunda, W.G. and Huntsman, S.A. (1997) Interrelated influence of iron, light and cell size on marine phytoplankton growth. Nature 390, 389-392.

Sunda, W.G. and Huntsman, S.A. (1998) Processes regulating cellular metal accumulation and physiological effects: phytoplankton as model systems. Science of The Total Environment 219, 165-181.

Sunda, W.G., Price, N.M. and Morel, F.M.M. (2005) Trace metal ion buffers and their use in culture studies, in: Andersen, R.A. (Ed.), Algal culturing techniques. Elsevier Academic Press, Burlington.

Tang, D. and Morel, F.M.M. (2006) Distinguishing between cellular and Fe-oxide-associated trace elements in phytoplankton. Marine Chemistry 98, 18-30.

Tovar-Sanchez, A., Sañudo-Wilhelmy, S.A., Garcia-Vargas, M., Weaver, R.S., Popels, L.C. and Hutchins, D.A. (2003) A trace metal clean reagent to remove surface-bound iron from marine phytoplankton. Marine Chemistry 82, 91-99.

Twining, B.S. and Baines, S.B. (2013) The trace metal composition of marine phytoplankton. Annual Review of Marine Science 5, 191-215.

Twining, B.S., Baines, S.B., Fisher, N.S., Maser, J., Vogt, S., Jacobsen, C., Tovar-Sanchez, A. and Sañudo-Wilhelmy, S.A. (2003) Quantifying trace elements in individual aquatic protist cells with a synchrotron X-ray fluorescence microprobe. Analytical Chemistry 75, 3806-3816.

Vance, D., Little, S.H., Archer, C., Cameron, V., Andersen, M.B., Rijkenberg, M.J.A. and Lyons, T.W. (2016a) The oceanic budgets of nickel and zinc isotopes: the importance of sulfidic environments as illustrated by the Black Sea. Philosophical Transactions of the Royal Society A: Mathematical, Physical and Engineering Sciences 374, 1-26.

Vance, D., Little, S.H., de Souza, G.F., Khatiwala, S., Lohan, M.C. and Middag, R. (2017) Silicon and zinc biogeochemical cycles coupled through the Southern Ocean. Nature Geoscience 10, 202-206.

Vance, D., Matthews, A., Keech, A., Archer, C., Hudson, G., Pett-Ridge, J. and Chadwick, O.A. (2016b) The behaviour of Cu and Zn isotopes during soil development: controls on the dissolved load of rivers. Chemical Geology 445, 36-53.

Wyatt, N.J., Milne, A., Woodward, E.M.S., Rees, A.P., Browning, T.J., Bouman, H.A., Worsfold, P.J. and Lohan, M.C. (2014) Biogeochemical cycling of dissolved zinc along the GEOTRACES South Atlantic transect GA10 at 40°S. Global Biogeochemical Cycles 28, 44-56.

Zhao, Y. (2011) The carbon cycle and bioactive trace metals in the oceans: constraints from zinc isotopes. PhD thesis, University of Bristol.

Zhao, Y., Vance, D. and Abouchami, W. (2011) Zinc isotopes in the southern ocean – a tracer of biogeochemical cycling?, Goldschmidt conference abstract, Prague, Czech Republic, p. 2266.

Zhao, Y., Vance, D., Abouchami, W. and de Baar, H.J.W. (2014) Biogeochemical cycling of zinc and its isotopes in the Southern Ocean. Geochimica et Cosmochimica Acta 125, 653-672.

# Figure captions

**Table 1.** Measured Fe and Zn uptake rates, cellular Zn quotas, and Zn isotope results ($\Delta^{66}Zn_{\text{biomass - medium}} = \delta^{66}Zn_{\text{biomass}} - \delta^{66}Zn_{\text{medium}}$) obtained for two different cultured marine diatoms. The specific growth rate (μ) has been suppressed to a different extent by the systematic variation of Fe′ at constant bioavailable Zn levels.

**Table 2.** Results of all non-linear Monod (1949), Michaelis-Menten (1913), and pseudo-Michaelis-Menten curve fits. The prefix 'pseudo' refers to the fact that the Michaelis-Menten equation is used to describe the Zn uptake rate as a function of Fe′, rather than the Fe uptake rate (*c.f.*, Figure 6). The superscript * refers to a previous fit result by Sunda and Huntsman (1997), which is here compared to an extended dataset, also including the new data reported here (Figure 2B).

**Figure 1.** Schematic illustration of Zn uptake into marine diatoms. Free Zn hexa-aquo complexes in the artificial seawater medium equilibrate with the transition metal buffer, here the organic chelator ethylenediaminetetraacetic acid (EDTA). The Zn fraction that is neither organically nor

929 inorganically complexed is considered available for uptake across the cell wall by active
930 transporters (Anderson et al., 1978). The rate limiting step in the uptake kinetics is considered to
931 be the dehydration of the hexa-aquo Zn to form an inner-sphere surface complex at the transporter
932 site (Hudson and Morel, 1990).

933 **Figure 2.** Specific growth rate (A) and surface area normalized Fe uptake rates (B) as a function
934 of the bioavailable Fe concentration (Fe′) in the culturing medium. A). The open ocean species
935 studied here are able to maintain higher growth rates at low Fe′ than the coastal diatoms
936 previously studied by Sunda and Huntsman (1997). B). The observed Fe uptake rates under
937 similar Fe′-limiting conditions were found to be in good agreement with this previous work.
938 Confidence (dark green) and prediction (light green) intervals of the previously published
939 relationship are given at significance levels of 95 %.

940 **Figure 3.** Distribution of Zn and its isotopes during uptake into cultured marine diatoms. A).
941 Zn/C ratios in this study compared to literature data (grey symbols and green curves). In the
942 present study, bioavailable Zn has been kept constant (vertical dashed blue line) at variable
943 degrees of Fe-limitation. The variability in C-normalized Zn quotas found here is larger than
944 previously reported (blue whisker) by Sunda and Huntsman (1992), and this variability is later
945 shown to be related to medium Fe′. The 25$^{th}$ and 75$^{th}$ percentiles of the dataset are marked by the
946 bottom and top edges of the blue whisker box, and the most extreme data points are given as
947 extended black lines and paler blue shading. B). Surface area normalized Zn uptake rate as a
948 function of the specific growth rate. The growth rate of *Chaetoceros sp.* is strongly suppressed
949 at low medium Fe′ (see later) and also generally showed surface area normalized Zn uptake rates
950 that were about half of those for *T. oceanica*. C). Zn isotope fractionation ($\Delta^{66}Zn_{\text{biomass - medium}}$ =
951 $\delta^{66}Zn_{\text{biomass}} - \delta^{66}Zn_{\text{medium}}$) as a function of surface area normalized Zn uptake rates. The generally
952 high Zn uptake rates found for *T. oceanica* consistently come with a 0.2 ‰ preference for light
953 isotopes associated with the biomass. The *Chaetoceros sp.* biomass was characterized by much
954 more variable signatures, with the most negative values at high Zn uptake rates and an increasing
955 preference for heavy Zn isotopes at lower uptake rates.

**Figure 4.** Interdependence of Zn and Fe uptake rates of two different cultured marine diatoms in the set of Fe′-limitation experiments undertaken in this study, all at constant bioavailable Zn.

**Figure 5.** The physiological interplay between Zn and Fe′ in two different cultured marine diatoms. A). P-normalized intracellular Zn quota as a function of Fe′. A few diatoms cultured at Fe′ levels higher than 0.7 nmol $l^{-1}$, a threshold above which Fe-hydroxides have previously been described to occur in culturing solutions (Sunda and Huntsman, 1995b, 1997), show increased Zn/P ratios. B). Zn and Fe uptake rates as a function of Fe′. The colored lines and band represent fits to the data using the Michaelis-Menten equation (*c.f.*, Section 4.2). Confidence (darker color) and prediction (brighter color) intervals of the given relationship are given at significance levels of 95 %, with the exception of the Fe prediction band, given at 75 %. Fe-limitation has been applied as an external forcing to reduce diatom growth, causing the steep decline in Fe uptake rates at low Fe′. C). The distribution of Zn isotopes with respect to the culturing medium, as a function of medium Fe′. The impact of Zn adsorption to Fe-hydroxides is illustrated by six culturing replicates conducted above the threshold of 0.7 nmol $l^{-1}$ Fe′. Positive Zn isotope signatures associated with *Chaetoceros sp.* are unlikely to be caused by adsorption to Fe-hydroxides in these Fe′-limitation experiments, as increasingly heavy signatures were consistently recorded away from the threshold for precipitation.

**Figure 6.** Cellular Zn quotas over a range of different Fe′-limiting conditions. A). The relationship between the specific growth rate and Fe′ for two different cultured marine diatoms, described by the Monod equation (Monod, 1949). B). Data for Zn uptake rates as a function of Fe′ are fitted using pseudo-Michaelis-Menten kinetics, which differs from the original equation in that the Zn uptake rate is described as function of Fe′ rather than of bioavailable Zn (Michaelis and Menten, 1913). This approach is unusual, but justification for doing so comes from the tight coupling of Zn and Fe uptake rates as presented in Figure 4. C). Intracellular Zn quotas predicted by the Droop equation from specific growth rates and Zn uptake rates. The numbers beside the curves show the changes in calculated Zn quotas as Fe′ decreases from optimal to severely Fe-limiting levels.

983 **Figure 7.** Schematic illustration of proposed Zn isotope effects associated with uptake into
984 cultured marine diatoms. A). Overview of the described effects as a function of the Zn uptake
985 rate. B). If the dehydration of the hexa-aquo Zn to form an inner-sphere surface complex at the
986 transporter site is the rate limiting step in the uptake kinetics (Hudson, 1998; Hudson and Morel,
987 1990; Sunda and Huntsman, 1998), light isotopes are expected to undergo this transformation
988 slightly faster than heavy Zn (Bigeleisen and Wolfsberg, 1958; Schauble, 2004; and references
989 therein). The maximum preference for light isotopes is achieved as soon as the cellular Zn uptake
990 rate exceeds the water loss rate at the transporter site. An increasing number of enzymes, per unit
991 area of cell wall, facilitates higher Zn uptake rates, whereas the dehydration at every single
992 transporter site is running at its maximum value with constant Zn isotope fractionation. C). If the
993 cellular Zn uptake rate is down-regulated to values lower than the dehydration rate of the Zn
994 hexa-aquo complex, the preference for light isotopes at the transporter becomes progressively
995 less important, and the biomass signature become isotopically heavier. In other words, conditions
996 close to those of an equilibrium situation between the free and surface bound Zn are established
997 at low Zn uptake rates, significantly lower than the water loss rate. Preferential uptake of heavy
998 Zn isotopes, under conditions that develop towards equilibrium at the transporter site with
999 decreasing Zn uptake rates, are consistent with many organic ligands that might form the active
1000 site of this enzyme (Ban et al., 2002; Fujii et al., 2014; Jouvin et al., 2009). D). In the experimental
1001 setup documented here, suppressed Zn uptake rates were promoted by reducing the availability
1002 Fe to the phytoplankton cell.

1003 **Figure A.1.** Cellular relationship between Zn/C ratios and bioavailable $Zn^{2+}$. A). Literature data
1004 for various phytoplankton species (Sunda and Huntsman, 1992). B). Schematic illustration on
1005 how this dataset can be interpreted as evidence for two distinct uptake mechanisms of high- and
1006 low-affinity. A second, additional, uptake mechanism (low-affinity) is turned on as soon as the
1007 high-affinity pathway reaches its maximum level of saturation.

1008 **Figure A.2.** Cellular relationship between Zn/C ratios and bioavailable $Zn^{2+}$ in a linear (left
1009 column) and logarithmic (right column) representation. Literature data for various phytoplankton

species (Sunda and Huntsman, 1992) are re-evaluated using an incremental curve-fitting approach. In this approach curve fits have been obtained with incrementally fewer data included in the evaluation scheme. The root mean squared error of the Michaelis-Menten equation has been used as an evaluation criterion to assess the goodness of fit. The literature dataset from its minimum value up to a $Zn^{2+}$ concentration of 1 nmol $l^{-1}$ has been included in the first curve fit (A and B). Starting from the same minimum value concentrations up to a $Zn^{2+}$ concentrations of 0.3 nmol $l^{-1}$ (C and D) and up to 0.1 nmol $l^{-1}$ (E and F) were included in the latter two calculations. Confidence (dark green) and prediction (light green) intervals of the relationships are given at significance levels of 95%, in addition to the solution of the Michaelis-Menten equation (red line). The whisker (blue) is identical to that given in Figure 3A and shows the $Zn^{2+}$ concentration used in this study.

# Figure 1

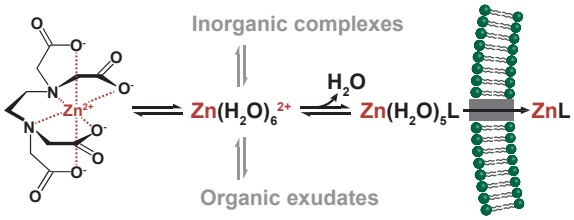
Inorganic complexes
Zn(H2O)6 2+
H2O
Zn(H2O)5L
ZnL
Organic exudates

# Figure 2

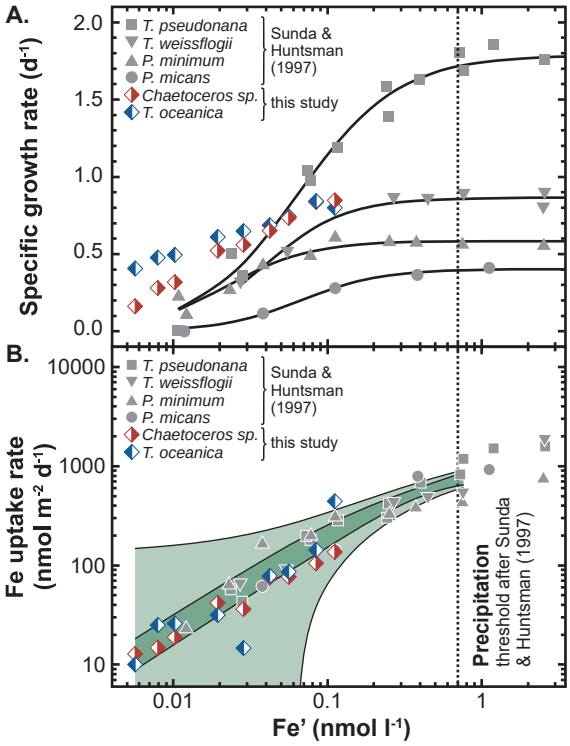
A.
Specific growth rate (d-1)
2.0
1.5
1.0
0.5
0.0
T. pseudonana
T. weissflogii
P. minimum
P. micans
Chaetoceros sp.
T. oceanica
Sunda & Huntsman (1997)
this study
B.
Fe uptake rate (nmol m-2 d-1)
10000
1000
100
10
0.01
0.1
1
Fe' (nmol l-1)
Precipitation
threshold after Sunda & Huntsman (1997)

# Figure 3

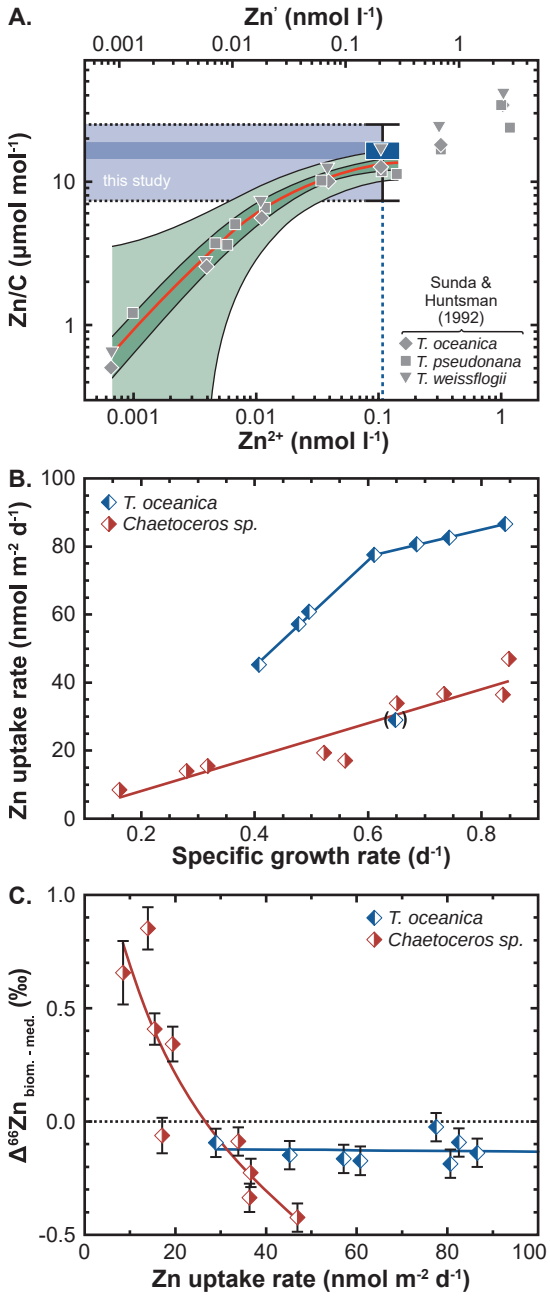
A.
Zn' (nmol l-1)
0.001
0.01
0.1
1
Zn/C (µmol mol-1)
10
1
this study
Sunda & Huntsman (1992)
T. oceanica
T. pseudonana
T. weissflogii
Zn2+ (nmol l-1)
B.
T. oceanica
Chaetoceros sp.
Zn uptake rate (nmol m-2 d-1)
100
80
60
40
20
0
0.2
0.4
0.6
0.8
Specific growth rate (d-1)
C.
T. oceanica
Chaetoceros sp.
Δ66Zn biom. - med. (‰)
1.0
0.5
0.0
-0.5
0
20
40
60
80
100
Zn uptake rate (nmol m-2 d-1)

# Figure 4

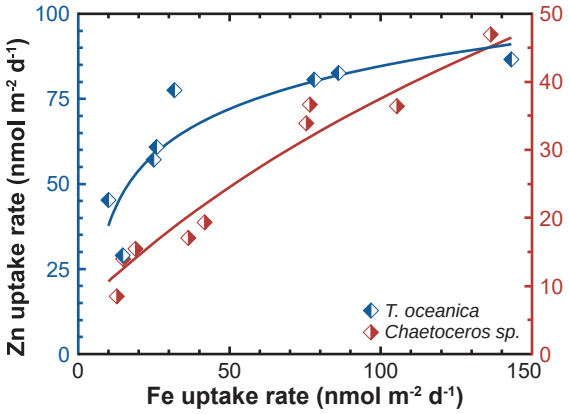
100
75
50
25
0
50
40
30
20
10
0
0
50
100
150
Zn uptake rate (nmol m-2 d-1)
Fe uptake rate (nmol m-2 d-1)
T. oceanica
Chaetoceros sp.

# Figure 5

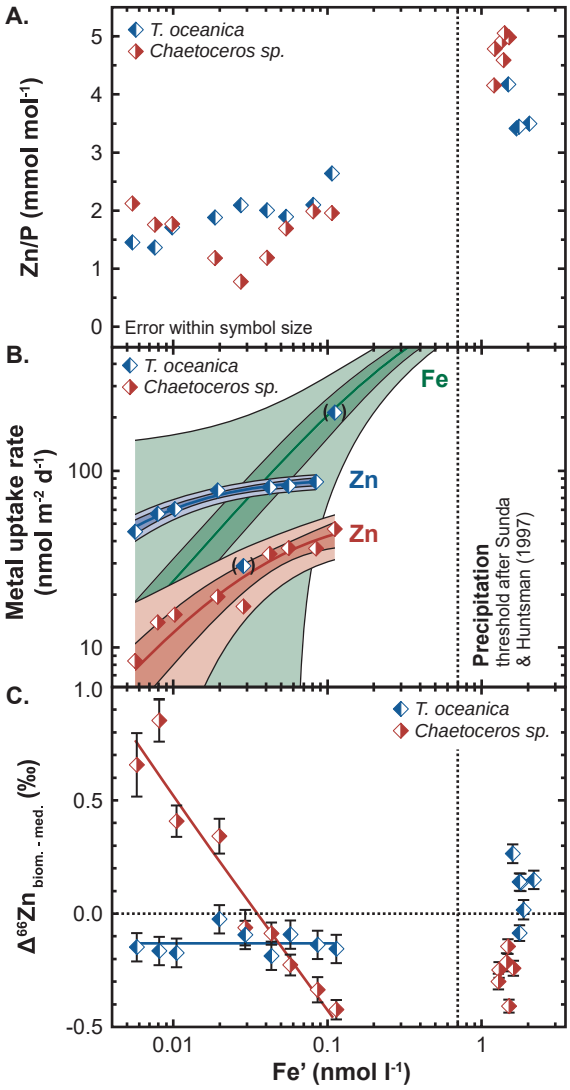
A.
T. oceanica
Chaetoceros sp.
Zn/P (mmol mol-1)
Error within symbol size
B.
T. oceanica
Chaetoceros sp.
Fe
Zn
Zn
Metal uptake rate (nmol m-2 d-1)
Precipitation
threshold after Sunda & Huntsman (1997)
C.
T. oceanica
Chaetoceros sp.
Δ66Zn biom. - med. (‰)
Fe' (nmol l-1)

# Figure 6

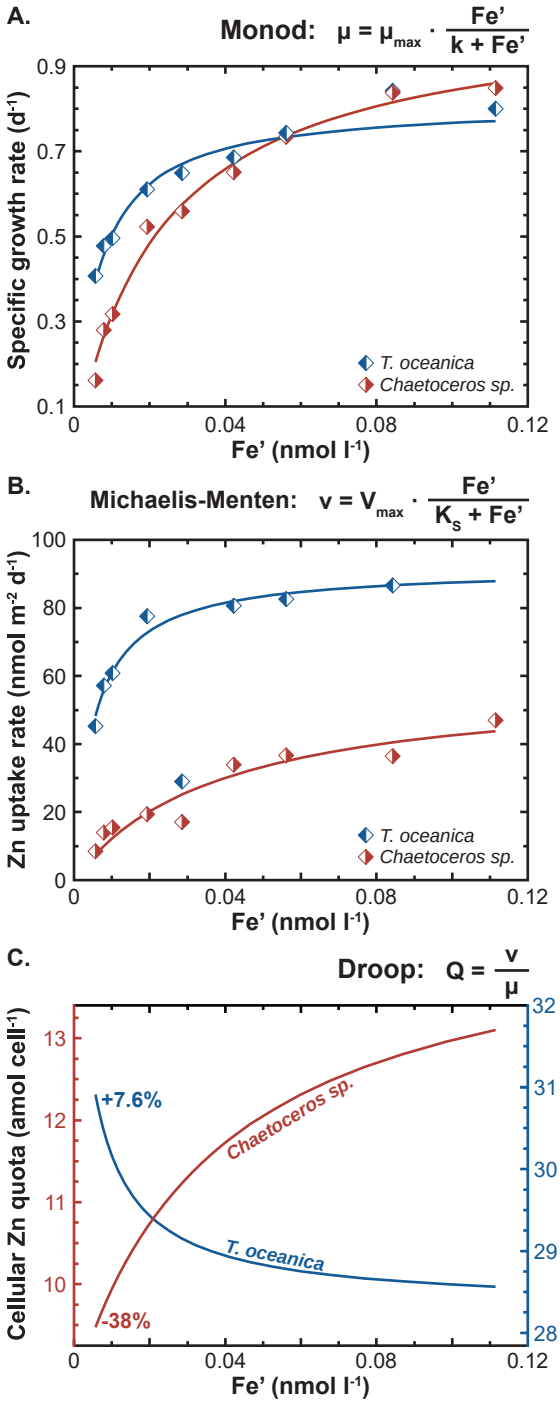
A.
Monod: μ = μmax · Fe' / (k + Fe')
Specific growth rate (d-1)
0.9
0.7
0.5
0.3
0.1
0
0.04
0.08
0.12
Fe' (nmol l-1)
T. oceanica
Chaetoceros sp.
B.
Michaelis-Menten: v = Vmax · Fe' / (Ks + Fe')
Zn uptake rate (nmol m-2 d-1)
100
80
60
40
20
0
0.04
0.08
0.12
Fe' (nmol l-1)
T. oceanica
Chaetoceros sp.
C.
Droop: Q = v / μ
Cellular Zn quota (amol cell-1)
13
12
11
10
32
31
30
29
28
+7.6%
-38%
Chaetoceros sp.
T. oceanica
0
0.04
0.08
0.12
Fe' (nmol l-1)

# Figure 7

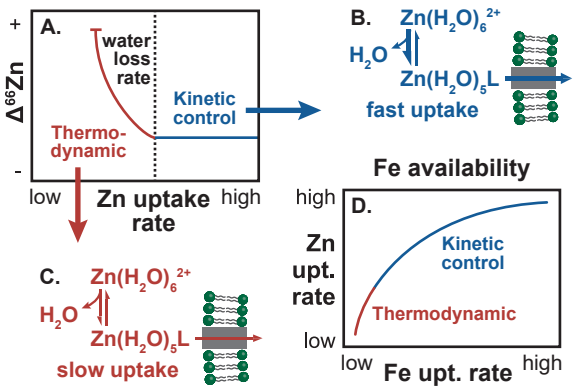
A.
water loss rate
Kinetic control
Thermo-dynamic
+
-
Δ66Zn
low
Zn uptake rate
high
B.
Zn(H2O)6 2+
H2O
Zn(H2O)5L
fast uptake
C.
Zn(H2O)6 2+
H2O
Zn(H2O)5L
slow uptake
Fe availability
high
D.
Zn upt. rate
Kinetic control
Thermodynamic
low
low
Fe upt. rate
high

# Table 1

| | Fe' | μ | Uptake rates | | Cellular Zn quotas | | | $\Delta^{66}Zn \pm 2\sigma$ (biom. - med.) |
|---|---|---|---|---|---|---|---|---|
| | | | Fe | Zn | Zn/C | Zn/P | Droop | |
| ***T. oceanica*** | 0.006 | 0.41 | 10.0 | 45.2 | 13.7 | 1.45 | 30.9 | -0.15 ± 0.04 |
| | 0.008 | 0.48 | 24.9 | 57.2 | 12.9 | 1.36 | 30.5 | -0.17 ± 0.04 |
| | 0.010 | 0.50 | 25.8 | 60.8 | 16.1 | 1.71 | 30.1 | -0.17 ± 0.05 |
| | 0.019 | 0.61 | 31.8 | 77.5 | 17.7 | 1.88 | 29.5 | -0.02 ± 0.04 |
| | 0.029 | 0.65 | 14.7 | 28.9 | 19.8 | 2.09 | 29.2 | -0.09 ± 0.05 |
| | 0.042 | 0.69 | 78.0 | 80.7 | 18.9 | 2.01 | 28.9 | -0.19 ± 0.05 |
| | 0.056 | 0.74 | 86.1 | 82.5 | 17.8 | 1.89 | 28.8 | -0.09 ± 0.05 |
| | 0.084 | 0.84 | 143.2 | 86.6 | 19.8 | 2.10 | 28.6 | -0.14 ± 0.04 |
| | 0.112 | 0.80 | 441.2 | 213.1 | 24.9 | 2.64 | 28.6 | -0.16 ± 0.04 |
| | 1.55 | - | - | - | - | 4.2 | - | 0.26 ± 0.04 |
| | 1.72 | - | - | - | - | 3.6 | - | -0.09 ± 0.03 |
| | 1.72 | - | - | - | - | 3.7 | - | 0.14 ± 0.04 |
| | 1.76 | - | - | - | - | 3.4 | - | 0.14 ± 0.04 |
| | 1.82 | - | - | - | - | 3.4 | - | 0.02 ± 0.04 |
| | 2.13 | - | - | - | - | 3.5 | - | 0.15 ± 0.04 |
| ***Chaetoceros sp.*** | 0.006 | 0.16 | 12.8 | 8.44 | 20.0 | 2.12 | 9.5 | 0.66 ± 0.14 |
| | 0.008 | 0.28 | 14.9 | 13.9 | 16.6 | 1.76 | 9.7 | 0.85 ± 0.09 |
| | 0.010 | 0.32 | 18.9 | 15.4 | 16.7 | 1.77 | 10.0 | 0.41 ± 0.07 |
| | 0.019 | 0.52 | 41.8 | 19.4 | 11.1 | 1.18 | 10.7 | 0.34 ± 0.08 |
| | 0.029 | 0.56 | 36.4 | 17.1 | 7.36 | 0.78 | 11.2 | -0.06 ± 0.08 |
| | 0.042 | 0.65 | 75.4 | 33.9 | 11.2 | 1.19 | 11.8 | -0.09 ± 0.05 |
| | 0.056 | 0.73 | 76.6 | 36.7 | 16.0 | 1.69 | 12.2 | -0.23 ± 0.05 |
| | 0.084 | 0.84 | 105.4 | 36.4 | 18.8 | 1.99 | 12.8 | -0.34 ± 0.06 |
| | 0.112 | 0.85 | 136.3 | 46.9 | 18.5 | 1.96 | 13.1 | -0.42 ± 0.04 |
| | 1.26 | - | - | - | - | 4.2 | - | -0.30 ± 0.03 |
| | 1.27 | - | - | - | - | 4.8 | - | -0.25 ± 0.03 |
| | 1.42 | - | - | - | - | 4.9 | - | -0.21 ± 0.04 |
| | 1.44 | - | - | - | - | 4.6 | - | -0.14 ± 0.03 |
| | 1.47 | - | - | - | - | 5.1 | - | -0.41 ± 0.03 |
| | 1.57 | - | - | - | - | 5.0 | - | -0.24 ± 0.03 |
| | $nmol\ l^{-1}$ | $d^{-1}$ | $nmol\ m^{-2}\ d^{-1}$ | $nmol\ m^{-2}\ d^{-1}$ | $\mu mol\ mol^{-1}$ | $mmol\ mol^{-1}$ | $amol\ cell^{-1}$ | ‰ |

# Table 2

| $a \cdot \frac{Fe'}{b + Fe'}$ | Fit results | | $R^2_{adj.}$ |
|---|---|---|---|
| | a | b | |
| **Monod** | $\mu_{max}$ | $k$ | |
| *T. oceanica* | 0.81 ± 0.04 | 0.006 ± 0.001 | 0.975 |
| *Chaetoceros sp.* | 1.04 ± 0.08 | 0.023 ± 0.004 | 0.987 |
| **Michaelis-Menten** | $V_{max}$ | $K_S$ | |
| Fe(Fe'), previous* | 1276 | 0.51 | n.a. |
| Fe(Fe'), this study | 1289 ± 263 | 0.53 ± 0.19 | 0.803 |
| **Zn(Fe') - kinetics** | $V_{max}$ | $K_S$ | |
| *T. oceanica* | 91.9 ± 2.2 | 0.005 ± 0.001 | 0.968 |
| *Chaetoceros sp.* | 58.9 ± 8.6 | 0.038 ± 0.013 | 0.896 |
| | nmol $m^{-2}$ $d^{-1}$ | nmol $l^{-1}$ | |

# Figure A.1

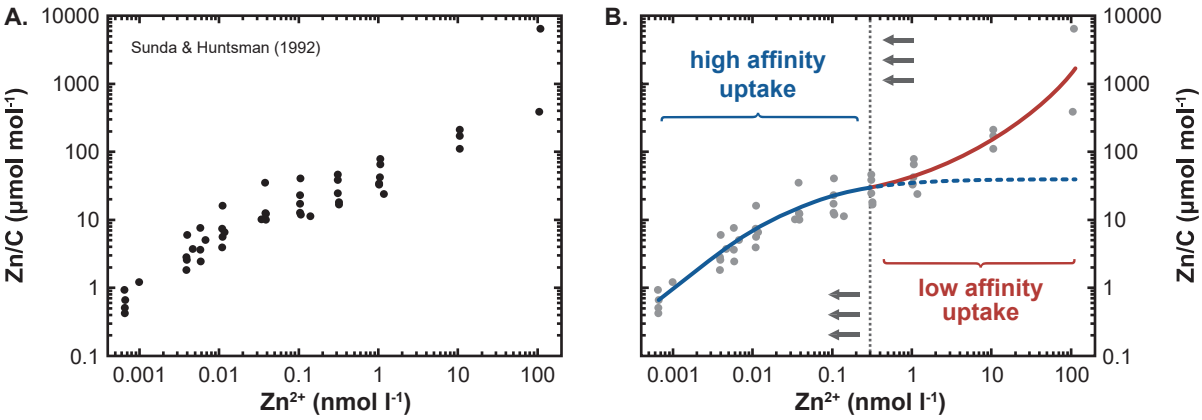
A.
Sunda & Huntsman (1992)
Zn/C (µmol mol-1)
Zn2+ (nmol l-1)
B.
high affinity uptake
low affinity uptake
Zn/C (µmol mol-1)
Zn2+ (nmol l-1)

# Figure A.2

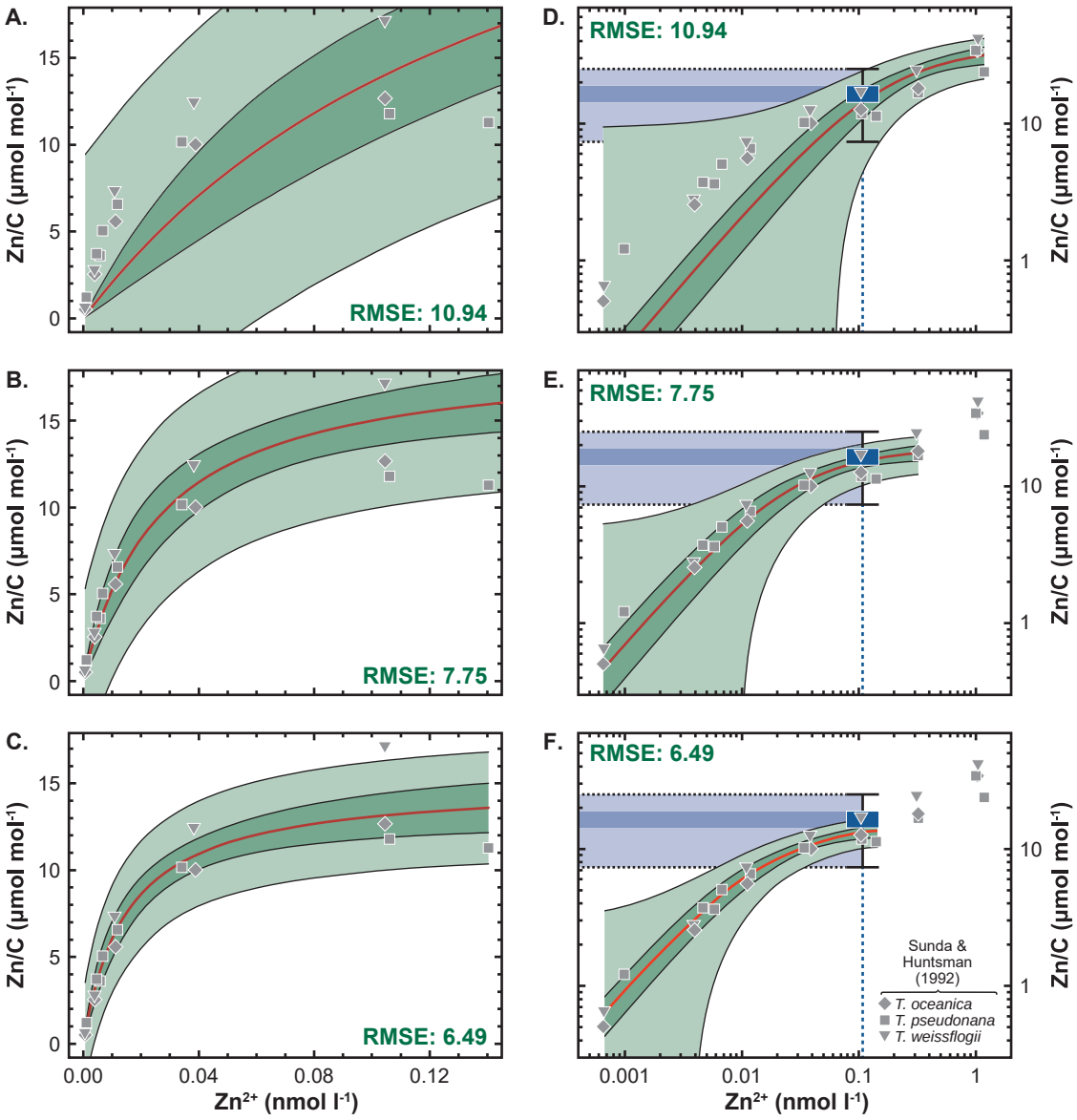
A.
B.
C.
D.
E.
F.
RMSE: 10.94
RMSE: 7.75
RMSE: 6.49
Zn/C (µmol mol⁻¹)
Zn²⁺ (nmol l⁻¹)
0
5
10
15
0.00
0.04
0.08
0.12
1
10
0.001
0.01
0.1
1
Sunda & Huntsman (1992)
T. oceanica
T. pseudonana
T. weissflogii

**table 1**

| | Fe' | μ | Uptake rates | | Cellular Zn quotas | | | $\Delta^{66}Zn \pm 2\ \sigma$ (biom. - med.) |
|---|---|---|---|---|---|---|---|---|
| | | | Fe | Zn | Zn/C | Zn/P | Droop | |
| ***T. oceanica*** | 0.006 | 0.41 | 10.0 | 45.2 | 13.7 | 1.45 | 30.9 | -0.15 ± 0.04 |
| | 0.008 | 0.48 | 24.9 | 57.2 | 12.9 | 1.36 | 30.5 | -0.17 ± 0.04 |
| | 0.010 | 0.50 | 25.8 | 60.8 | 16.1 | 1.71 | 30.1 | -0.17 ± 0.05 |
| | 0.019 | 0.61 | 31.8 | 77.5 | 17.7 | 1.88 | 29.5 | -0.02 ± 0.04 |
| | 0.029 | 0.65 | 14.7 | 28.9 | 19.8 | 2.09 | 29.2 | -0.09 ± 0.05 |
| | 0.042 | 0.69 | 78.0 | 80.7 | 18.9 | 2.01 | 28.9 | -0.19 ± 0.05 |
| | 0.056 | 0.74 | 86.1 | 82.5 | 17.8 | 1.89 | 28.8 | -0.09 ± 0.05 |
| | 0.084 | 0.84 | 143.2 | 86.6 | 19.8 | 2.10 | 28.6 | -0.14 ± 0.04 |
| | 0.112 | 0.80 | 441.2 | 213.1 | 24.9 | 2.64 | 28.6 | -0.16 ± 0.04 |
| | 1.55 | - | - | - | - | 4.2 | - | 0.26 ± 0.04 |
| | 1.72 | - | - | - | - | 3.6 | - | -0.09 ± 0.03 |
| | 1.72 | - | - | - | - | 3.7 | - | 0.14 ± 0.04 |
| | 1.76 | - | - | - | - | 3.4 | - | 0.14 ± 0.04 |
| | 1.82 | - | - | - | - | 3.4 | - | 0.02 ± 0.04 |
| | 2.13 | - | - | - | - | 3.5 | - | 0.15 ± 0.04 |
| ***Chaetoceros sp.*** | 0.006 | 0.16 | 12.8 | 8.44 | 20.0 | 2.12 | 9.5 | 0.66 ± 0.14 |
| | 0.008 | 0.28 | 14.9 | 13.9 | 16.6 | 1.76 | 9.7 | 0.85 ± 0.09 |
| | 0.010 | 0.32 | 18.9 | 15.4 | 16.7 | 1.77 | 10.0 | 0.41 ± 0.07 |
| | 0.019 | 0.52 | 41.8 | 19.4 | 11.1 | 1.18 | 10.7 | 0.34 ± 0.08 |
| | 0.029 | 0.56 | 36.4 | 17.1 | 7.36 | 0.78 | 11.2 | -0.06 ± 0.08 |
| | 0.042 | 0.65 | 75.4 | 33.9 | 11.2 | 1.19 | 11.8 | -0.09 ± 0.05 |
| | 0.056 | 0.73 | 76.6 | 36.7 | 16.0 | 1.69 | 12.2 | -0.23 ± 0.05 |
| | 0.084 | 0.84 | 105.4 | 36.4 | 18.8 | 1.99 | 12.8 | -0.34 ± 0.06 |
| | 0.112 | 0.85 | 136.3 | 46.9 | 18.5 | 1.96 | 13.1 | -0.42 ± 0.04 |
| | 1.26 | - | - | - | - | 4.2 | - | -0.30 ± 0.03 |
| | 1.27 | - | - | - | - | 4.8 | - | -0.25 ± 0.03 |
| | 1.42 | - | - | - | - | 4.9 | - | -0.21 ± 0.04 |
| | 1.44 | - | - | - | - | 4.6 | - | -0.14 ± 0.03 |
| | 1.47 | - | - | - | - | 5.1 | - | -0.41 ± 0.03 |
| | 1.57 | - | - | - | - | 5.0 | - | -0.24 ± 0.03 |
| | nmol $l^{-1}$ | $d^{-1}$ | nmol $m^{-2}$ $d^{-1}$ | nmol $m^{-2}$ $d^{-1}$ | μmol $mol^{-1}$ | mmol $mol^{-1}$ | amol $cell^{-1}$ | ‰ |

table 2

| $a \cdot \frac{Fe'}{b + Fe'}$ | Fit results | | $R^2_{adj.}$ |
|---|---|---|---|
| | a | b | |
| **Monod** | $\mu_{max}$ | $k$ | |
| *T. oceanica* | 0.81 ± 0.04 | 0.006 ± 0.001 | 0.975 |
| *Chaetoceros sp.* | 1.04 ± 0.08 | 0.023 ± 0.004 | 0.987 |
| **Michaelis-Menten** | $V_{max}$ | $K_S$ | |
| Fe(Fe'), previous* | 1276 | 0.51 | n.a. |
| Fe(Fe'), this study | 1289 ± 263 | 0.53 ± 0.19 | 0.803 |
| **Zn(Fe') - kinetics** | $V_{max}$ | $K_S$ | |
| *T. oceanica* | 91.9 ± 2.2 | 0.005 ± 0.001 | 0.968 |
| *Chaetoceros sp.* | 58.9 ± 8.6 | 0.038 ± 0.013 | 0.896 |
| | nmol $m^{-2}$ $d^{-1}$ | nmol $l^{-1}$ | |

figure 1

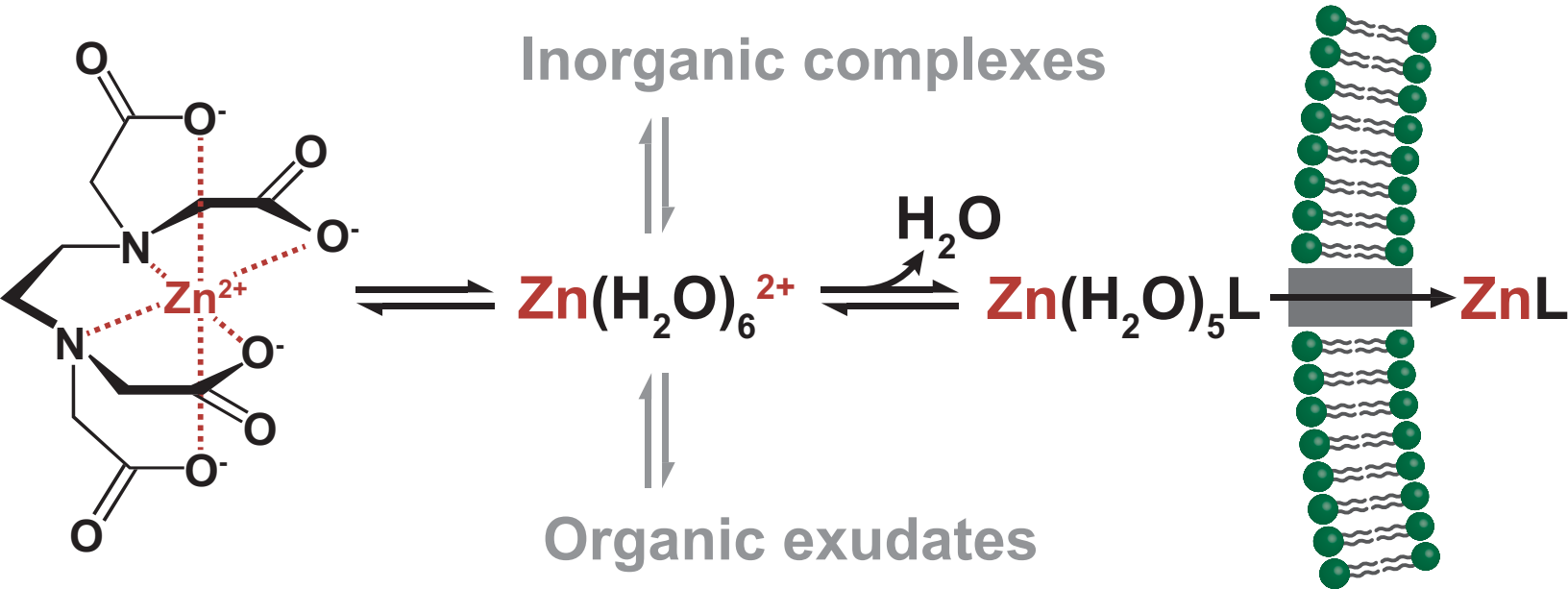
Inorganic complexes
Zn(H2O)6 2+
H2O
Zn(H2O)5L
ZnL
Organic exudates
Zn2+

Figure 2

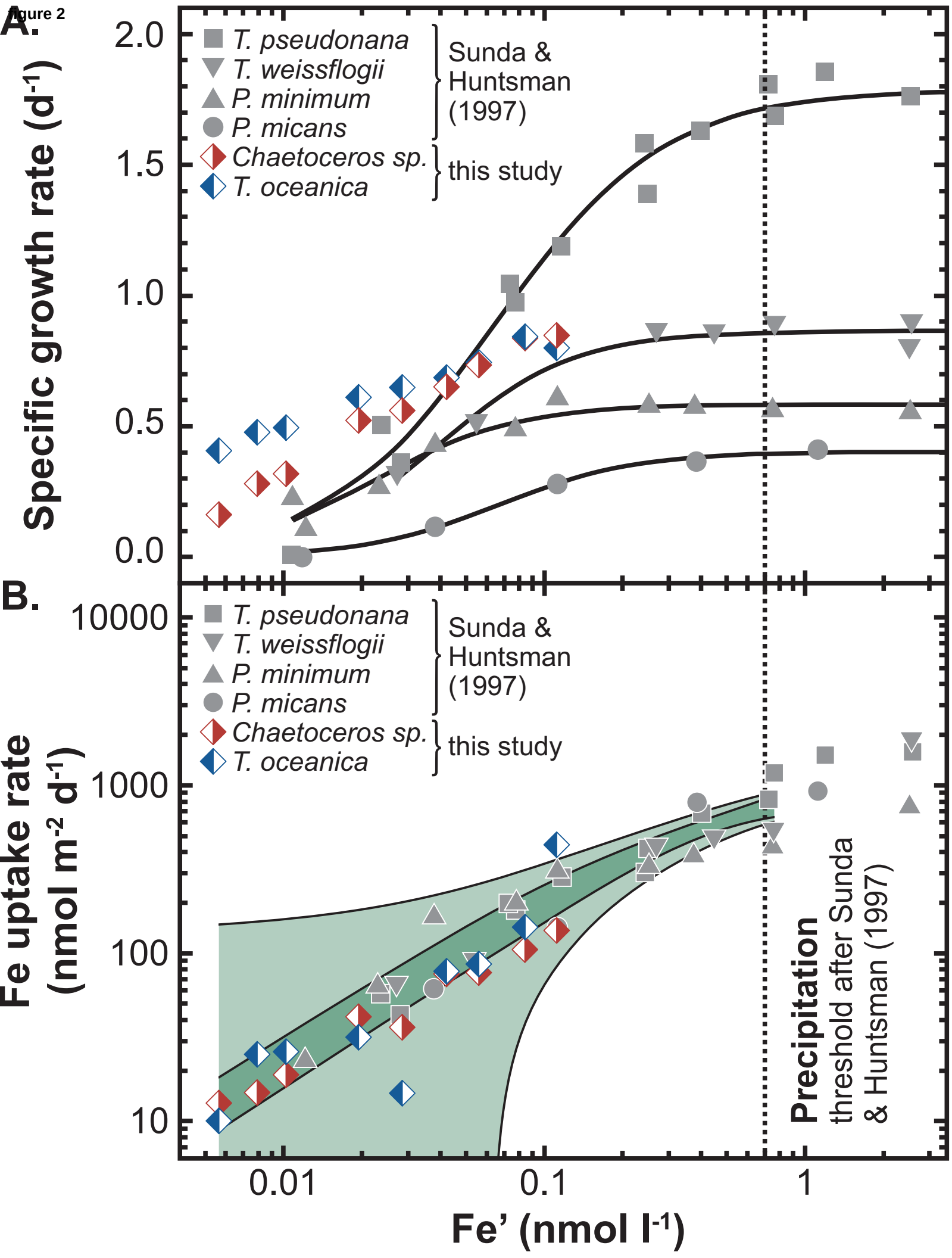
A.
Specific growth rate (d-1)
2.0
1.5
1.0
0.5
0.0
T. pseudonana
T. weissflogii
P. minimum
P. micans
Chaetoceros sp.
T. oceanica
Sunda & Huntsman (1997)
this study
B.
Fe uptake rate (nmol m-2 d-1)
10000
1000
100
10
0.01
0.1
1
Fe' (nmol l-1)
Precipitation
threshold after Sunda & Huntsman (1997)

figure 3

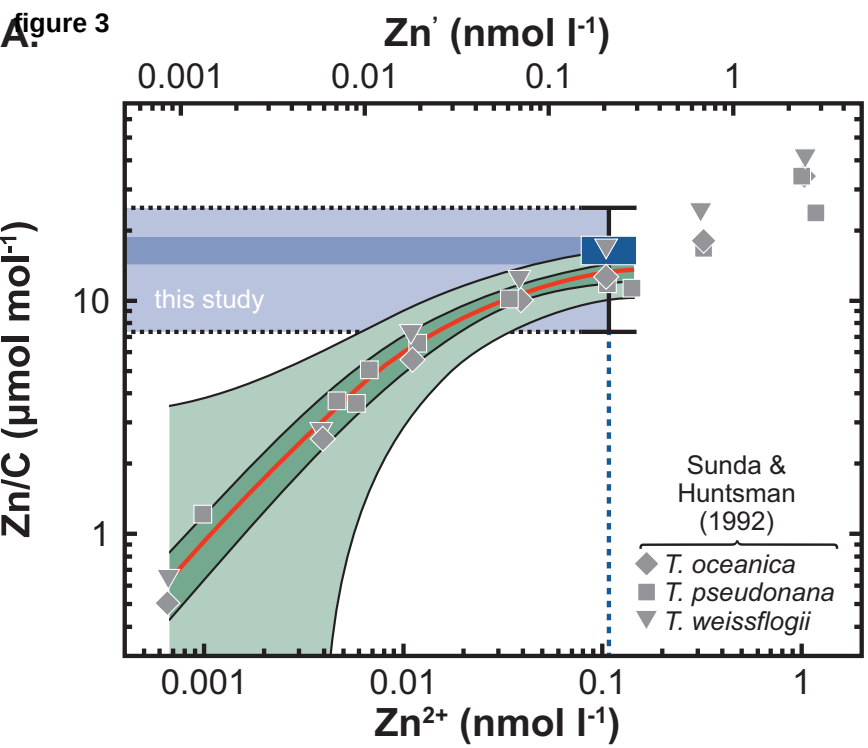
A.
Zn' (nmol l-1)
0.001
0.01
0.1
1
Zn/C (µmol mol-1)
10
1
this study
Sunda & Huntsman (1992)
T. oceanica
T. pseudonana
T. weissflogii
Zn2+ (nmol l-1)

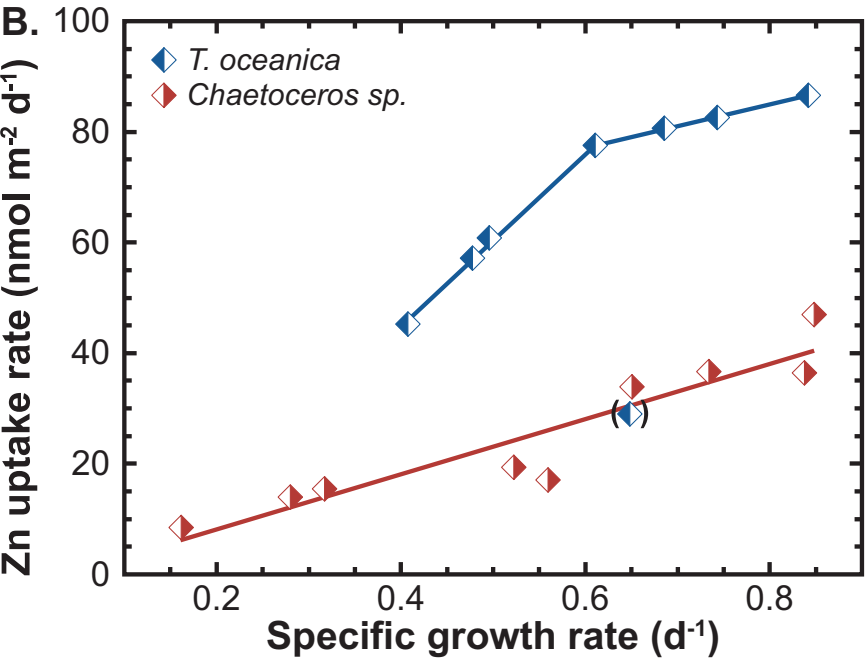
B.
Zn uptake rate (nmol m-2 d-1)
100
80
60
40
20
0
T. oceanica
Chaetoceros sp.
0.2
0.4
0.6
0.8
Specific growth rate (d-1)

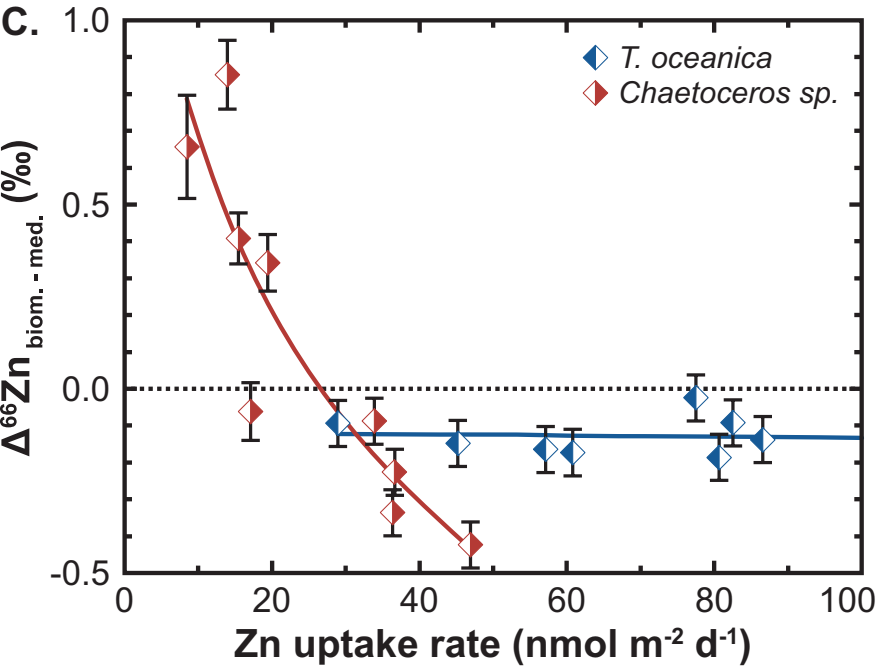
C.
Δ66Zn biom. - med. (‰)
1.0
0.5
0.0
-0.5
T. oceanica
Chaetoceros sp.
0
20
40
60
80
100
Zn uptake rate (nmol m-2 d-1)

figure 4

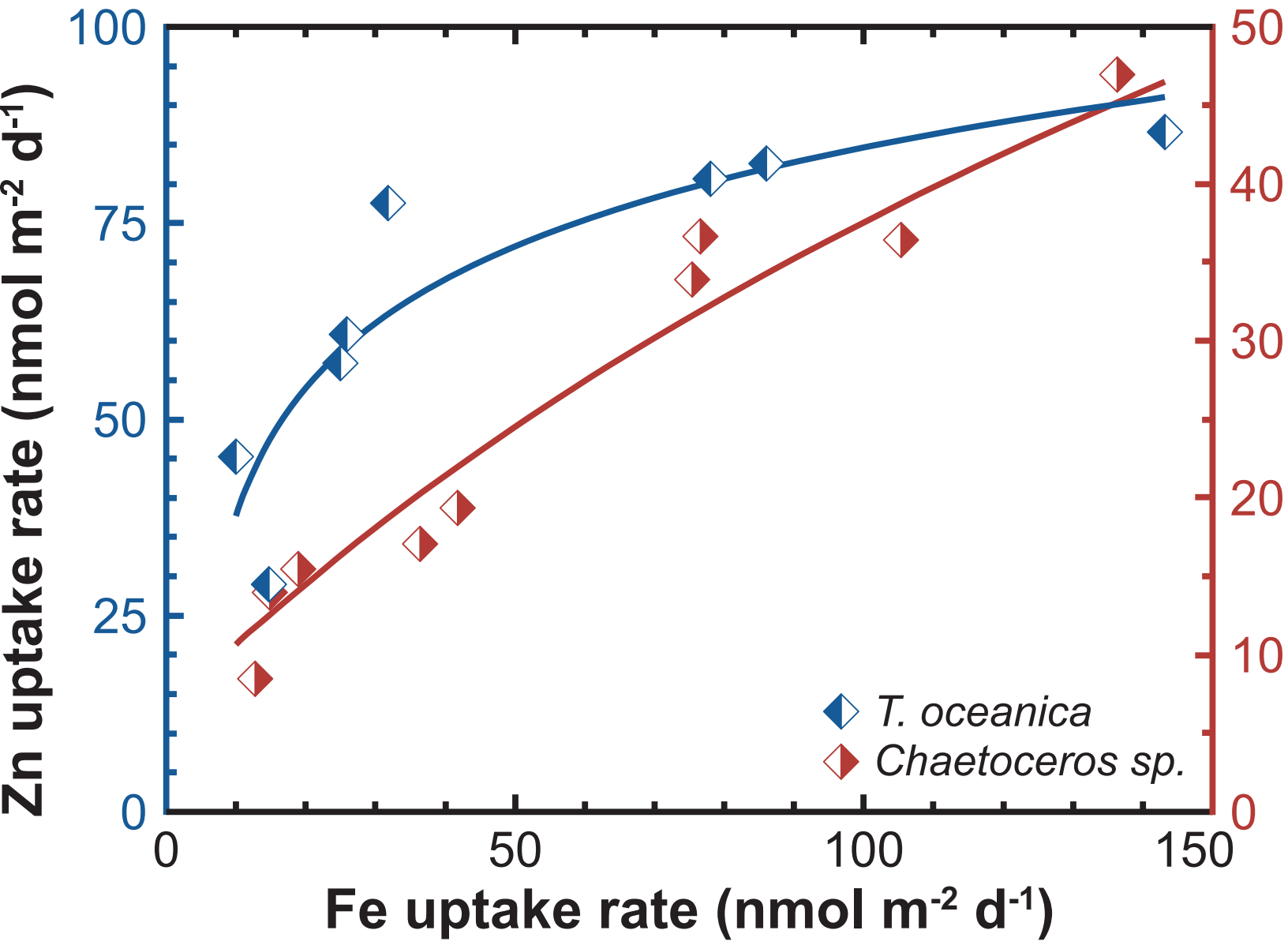
100
75
50
25
0
50
40
30
20
10
0
0
50
100
150
Zn uptake rate (nmol m-2 d-1)
Fe uptake rate (nmol m-2 d-1)
T. oceanica
Chaetoceros sp.

Figure 5

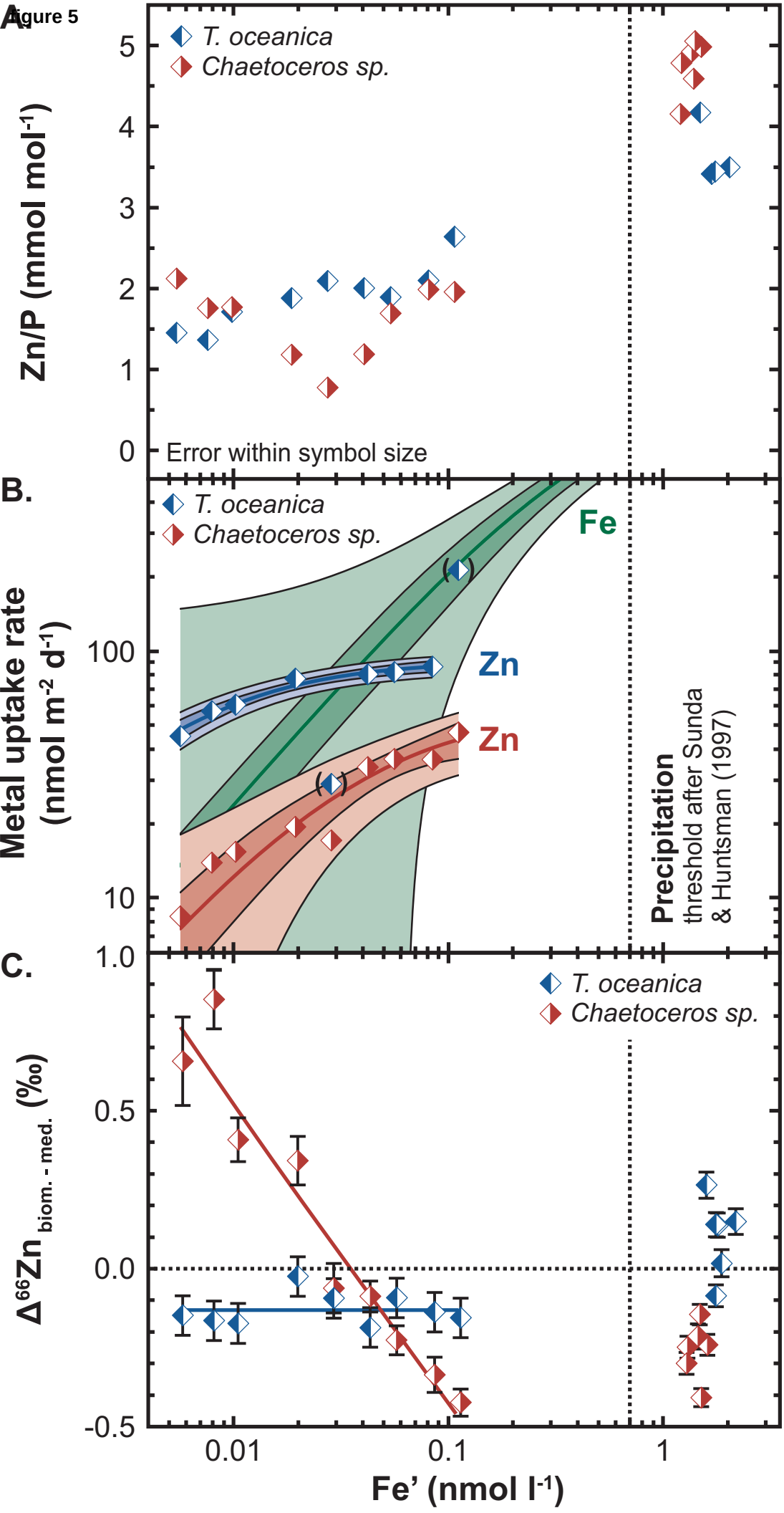
A.
T. oceanica
Chaetoceros sp.
Zn/P (mmol mol-1)
0
1
2
3
4
5
Error within symbol size
B.
T. oceanica
Chaetoceros sp.
Fe
Zn
Zn
Metal uptake rate (nmol m-2 d-1)
10
100
Precipitation
threshold after Sunda & Huntsman (1997)
C.
T. oceanica
Chaetoceros sp.
Δ66Zn biom. - med. (‰)
-0.5
0.0
0.5
1.0
0.01
0.1
1
Fe' (nmol l-1)

Figure 6

A.

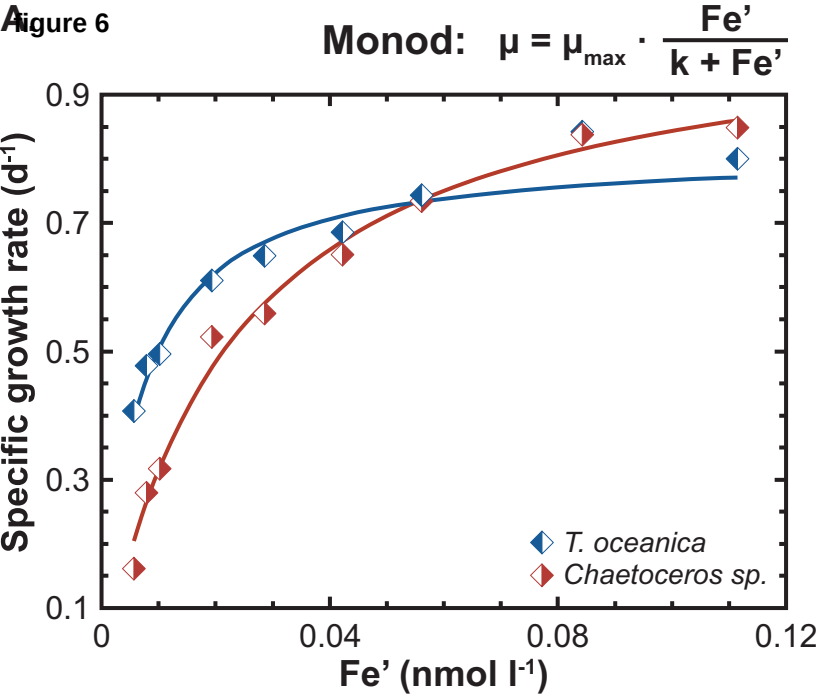
Monod: $\mu = \mu_{max} \cdot \frac{Fe'}{k + Fe'}$
Specific growth rate ($d^{-1}$)
0.9
0.7
0.5
0.3
0.1
0
0.04
0.08
0.12
Fe' (nmol $l^{-1}$)
T. oceanica
Chaetoceros sp.

B.

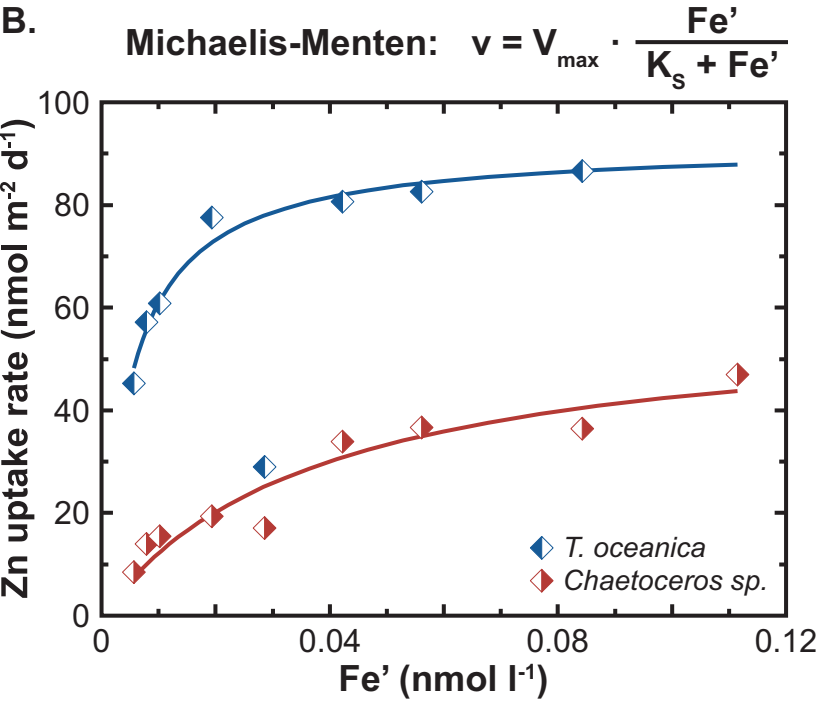
Michaelis-Menten: $v = V_{max} \cdot \frac{Fe'}{K_s + Fe'}$
Zn uptake rate (nmol $m^{-2}$ $d^{-1}$)
100
80
60
40
20
0
0.04
0.08
0.12
Fe' (nmol $l^{-1}$)
T. oceanica
Chaetoceros sp.

C.

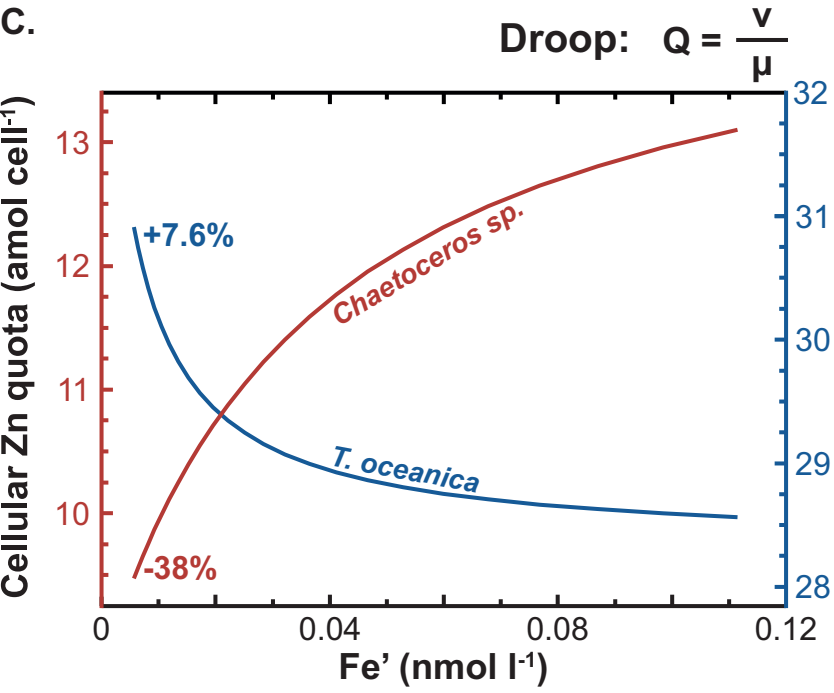
Droop: $Q = \frac{v}{\mu}$
Cellular Zn quota (amol $cell^{-1}$)
13
12
11
10
32
31
30
29
28
+7.6%
-38%
Chaetoceros sp.
T. oceanica
0
0.04
0.08
0.12
Fe' (nmol $l^{-1}$)

figure 7

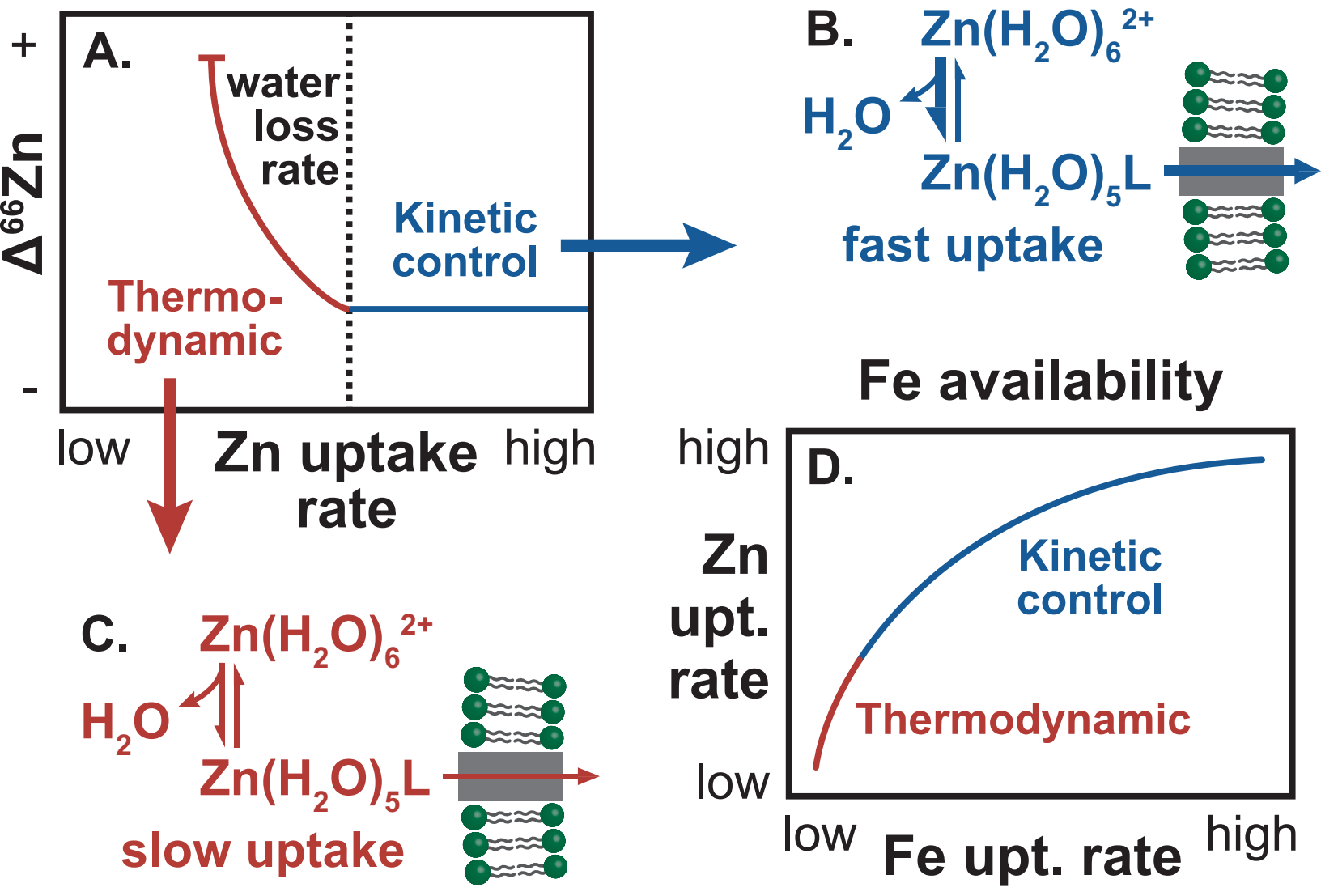
A.
water loss rate
Kinetic control
Thermo-dynamic
+
-
Δ66Zn
low
Zn uptake rate
high
B.
Zn(H2O)6 2+
H2O
Zn(H2O)5L
fast uptake
C.
Zn(H2O)6 2+
H2O
Zn(H2O)5L
slow uptake
Fe availability
high
Zn upt. rate
low
D.
Kinetic control
Thermodynamic
low
Fe upt. rate
high

figure A.1

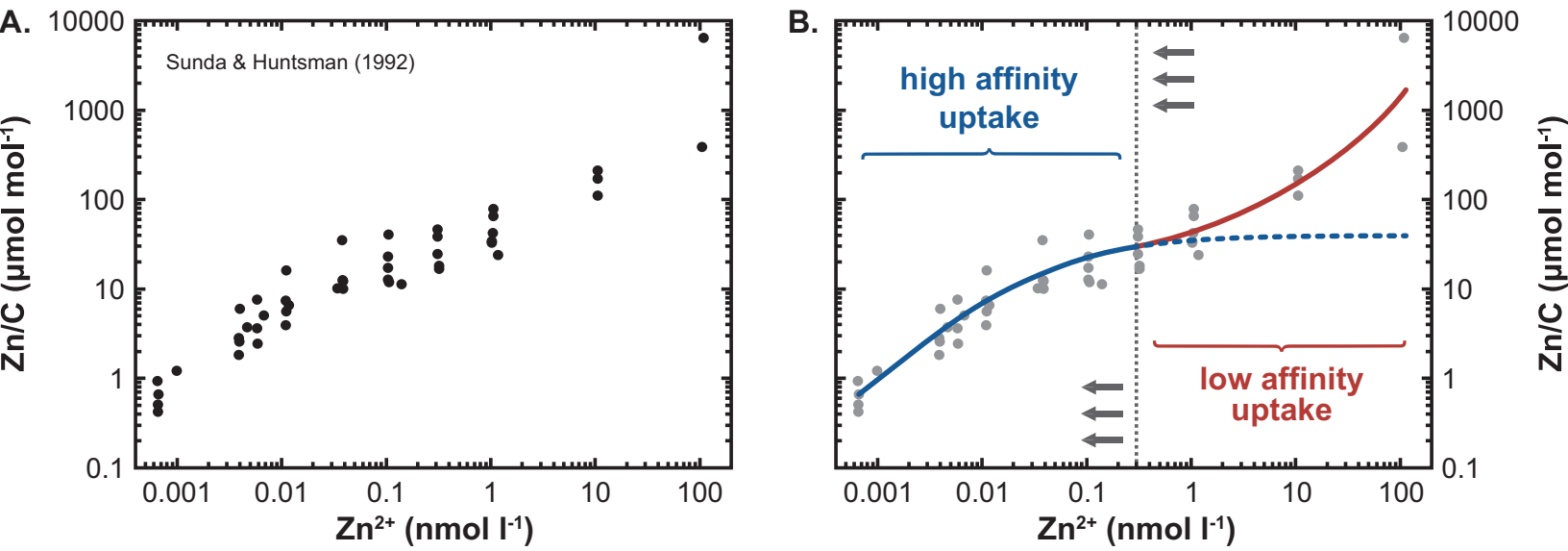
A.
Sunda & Huntsman (1992)
Zn/C (µmol mol-1)
Zn2+ (nmol l-1)
10000
1000
100
10
1
0.1
0.001
0.01
0.1
1
10
100
B.
high affinity uptake
low affinity uptake
Zn/C (µmol mol-1)
Zn2+ (nmol l-1)

figure A.2

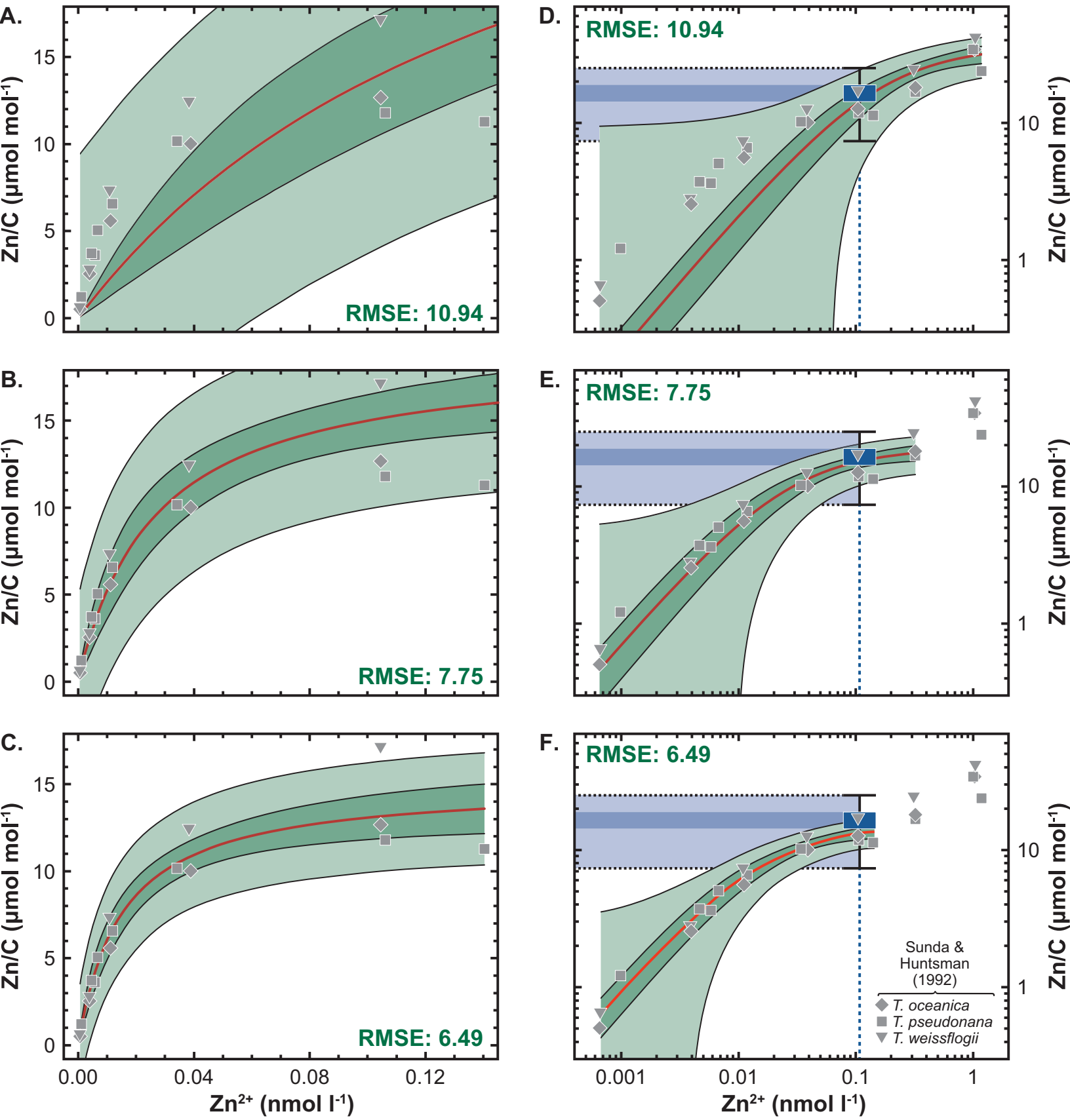
A.
B.
C.
D.
E.
F.
RMSE: 10.94
RMSE: 7.75
RMSE: 6.49
Zn/C (µmol mol-1)
Zn2+ (nmol l-1)
0.00
0.04
0.08
0.12
0.001
0.01
0.1
1
0
5
10
15
Sunda & Huntsman (1992)
T. oceanica
T. pseudonana
T. weissflogii